Angle Resolved Photoemission Calculations

Thesis by

Sarah A. Sheard

In Partial Fulfillment of the Requirements for the

Degree of Master of Science

California Institute of Technology
Pasadena, California

June 1979

(Submitted September 1, 1978)

to women in science

Acknowledgments

This thesis would not have been possible without the support and encouragement of my advisor, Dr. W. Henry Weinberg. Dr. Stephen L. Cunningham and Dr. John T. Yates were also invaluable for the theoretical and experimental portions of my work, respectively. I thank them all for their help. And I owe my sanity to two friends, Tom Stevens and my coworker Jenna Zinck; for their friendship I offer heartfeld thanks. To others, too numerous to mention individually, including the Booth Computing Center and the Noyes Glass Shop, my gratitude. I also thank Kathy Lewis for her excellent typing.

In addition, I would like to acknowledge the support of the Danforth and National Science Foundations for graduate fellowships and the National Science Foundation for research support.

Sally Sheard

Table of Contents

ANGLE-RESOLVED PHOTOEMISSION SPECTROSCOPY

INTRODUCTION

When high energy electromagnetic radiation interacts with molecules or solids, electrons are emitted. The study of these electrons is called photoelectron spectroscopy, or photoemission when dealing with metals. Angle-integrated photoelectron spectroscopy has been used routinely since the early sixties[1] to probe electronic states of molecules in the gas phase. Under such conditions, the random orientation of the molecules causes almost all angular dependences due to molecular properties to be averaged out. As a result, this technique produces peaks in electron intensity as a function of energy only, and is fairly straightforward to interpret. But a great deal of information is lost by this angular averaging.

Recently, interest has grown in extracting and analyzing this angular information. In order to measure angular dependences, one must first orient the molecules coherently. Hence, it becomes apparent that this technique is well suited to studying chemisorptive systems, where the metal surface orients the molecules by breaking the symmetry of their environment. In many cases, chemisorption perturbs the molecular orbital energies little enough that fruitful comparisons can be made with gas phase studies.

Furthermore, surface scientists have long been asking questions that angle-resolved photoemission is likely to help answer. Being more sensitive to the metal surface than to the bulk crystal, photoemission can

examine the admolecules while they are chemisorbed. Angle-integrated ultraviolet photoemission can determine the energetic positions of their valence orbitals but it can say very little, or nothing, about their bonding character, symmetry, or orientations. One must consider angular dependences to extract this information.

1. Previous Work

Interest in the application of angle-resolved photoelectron spectroscopy to chemisorption surged with the publication of a paper which calculated the spectrum expected from a single isolated CO molecule.[2] James Davenport used $X\alpha$ approximations for the initial state molecular orbitals and for the final state electron waves. Different angular distributions were calculated for different initial state orbitals. Such a calculation can be compared to measured photoemission distributions of any oriented CO molecules, and specifically to CO molecules adsorbed on metal surfaces. In the comparison, one could expect to find information on the "tip angles" of CO with respect to the surface, and on the extent of orbital mixing.

The subject of orbital mixing has been extensively pursued by J. W. Gadzuk.[3,4,5] Using Green's functions, he has studied the "surface-molecule" limit in which molecular orbitals of the adparticle mix with surface bands to produce a localized state called the surface-molecule. Photoemission from this state will then reflect this orbital mixing and can presumably be applied to distinguish "atop" sites from bridged and fourfold sites. Two major problems exist with his approach. One is that the final state is treated as a plane wave, which others[7] have shown

cannot reproduce experimental spectra. The second problem is that the extent of orbital mixing must be used as a parameter. This means distributions must be calculated with different values of the mixing parameter as well as of orbital energies and orientations. It is very difficult and time consuming to try to fit this many parameters to the experimental data.

A different approach was used by Liebsch,[8,9] and by Tong and Van Hove,[10] who account for the multiple scattering effects of the metal substrate. The electrons emitted from the adsorbate toward the metal are scattered and reflected back toward the detector, producing interference effects related to the symmetry of the surface. Although this approach best approximates the true final state of the electron, only atomic overlayers have been treated. Thus, initial state molecular orbitals have not been handled.

A synthesis of many of the above methods was provided by Jacobi, et al.[7] For an atom with two orbitals of symmetry a_1 and e, they tried several types of approximations, the best of which included LCAO initial state molecular orbitals and a LEED-type (scattered wave) final state. This approximation was compared to one with a plane wave final state and separately to one with an atomic-orbital initial state (no mixing). In the first case, the curves fit the experimental data quite well. In the other two, however, there was moderate to severe disagreement, particularly when the final state was a plane wave. Other papers of this group consider polarization changes, symmetry effects, and variations in $\underset{\sim}{A}$ at the surface,[11] and calculate distributions for a commonly encountered chemisorption system, CO on Ni(110).[12] The good agreement reached here between theory

and experiment paves the way for further studies of this type.

2. This Work

In our laboratory, we have currently the capability to perform angle-resolved photoemission experiments. We would like to analyze the experimental data by comparing it to theoretical curves calculated for a number of possible surface structures. In this way, we hope to use angle-resolved photoemission spectroscopy to deduce the configurations and properties of chemisorbed overlayers. For this reason, I have written a series of computer programs which calculate photoemission distributions from various atomic orbitals at arbitrary energies and polarizations. These programs and the writeups explaining specifically how each works are included in the appendix.

FORMALISM

Photoemission is treated here in the context of first order perturbation theory. The full Hamiltonian of the system is a sum of an unperturbed Hamiltonian and an interactional correction:

$$H = H^{(0)} + V, \tag{1}$$

where the perturbation V represents the interaction of the incident radiation with the admolecule plus substrate system. Classically, the full one-electron Hamiltonian can be written[13]

$$H = \frac{1}{2m}\left[\underset{\sim}{p} - \frac{e}{c}\underset{\sim}{A}(\underset{\sim}{r},t)\right]^2 + e\phi(\underset{\sim}{r},t) + v'(\underset{\sim}{r},t), \tag{2}$$

where $\underset{\sim}{p}$ is the momentum operator for the electron, $\underset{\sim}{A}$ is the vector potential of the radiation, ϕ is the scalar potential, and v' represents all potentials due to the unperturbed system. Expanding the square and removing the zeroth-order Hamiltonian, we have

$$V = \frac{-e}{2mc}\left[\underset{\sim}{p}\cdot\underset{\sim}{A} + \underset{\sim}{A}\cdot\underset{\sim}{p}\right] + \frac{e^2}{2mc^2}A^2 + e\phi\ . \tag{3}$$

Several assumptions will simplify this expression. If the wavelength of the radiative field is large with respect to the wavefunctions describing the system, then $\underset{\sim}{A}$ can be approximated as a constant using $e^{ik\cdot r} \sim 1$ (the dipole approximation). Then $\underset{\sim}{A}$ commutes with $\underset{\sim}{p}$, so that $\underset{\sim}{p}\cdot\underset{\sim}{A} = \underset{\sim}{A}\cdot\underset{\sim}{p}$. Since the perturbation, represented by $\underset{\sim}{A}$ is small, the A^2 term can be neglected, We can also set the scalar potential ϕ to zero since, in the absence of sources, one can always choose the Coulomb gauge. Then the perturbation is

simply $V = \frac{-e}{mc}(\underset{\sim}{A}\cdot\underset{\sim}{p})$.

It is desirable to transform the derivative operator $\underset{\sim}{p}$ to the multiplicative operator $\underset{\sim}{r}$. Using the fact that

$$[H,\underset{\sim}{r}] = H\underset{\sim}{r} - \underset{\sim}{r}H = \frac{ih}{m}\underset{\sim}{p}\ , \tag{4}$$

if the potential term v' does not depend on velocity, we find

$$V = \frac{-ie\hbar}{2m^2c}[\underset{\sim}{A}\cdot H\underset{\sim}{r} - \underset{\sim}{A}\cdot\underset{\sim}{r}H]\ . \tag{5}$$

Perturbation theory requires expanding the "true" perturbed states ψ in terms of the unperturbed eigenstates $\psi^{(0)}$. In this case, the expansion coefficients become

$$C_i = \frac{\langle\psi_f^{(0)}|V|\psi_i^{(0)}\rangle}{E_f - E_i}\ . \tag{6}$$

Substitution of Eq. (5) into the matrix element leads to an alternate expression for the perturbation:

$$V = \frac{-ie\hbar}{2m^2c}(E_f - E_i)(\underset{\sim}{A}\cdot\underset{\sim}{r})\ . \tag{7}$$

We must now find an expression which will incorporate the angular dependence of the photoemitted electrons into the transition probabilities. Assuming V is independent of time, we can use Fermi's Golden Rule for the transition rates:[13]

$$w = K|\langle\psi_f|A\cdot r|\psi_i\rangle|^2\ \rho_f(E_i^{(0)} + h\nu), \tag{8}$$

where we have substituted $\underset{\sim}{A}\cdot\underset{\sim}{r}$ for V, K represents a collection of constants, and energy conservation is accounted for by including the density of final states only at the energy of the initial state plus $h\nu$.

Now what we seek is the total final state wavefunction, which includes angular information. If the total final state wavefunction is denoted by ψ, the quantity

$$|\psi_f(\theta,\phi)|^2 \tag{9}$$

tells us the electron current reaching a detector located at (θ,ϕ) per unit time (since we are only interested in the angular dependences, and not in the absolute magnitudes of this function, we can neglect normalization and constants). This total wavefunction is a sum of the final states which are represented in Eq. (8). The sum must weigh these final states ϕ_f according to their likelihood of being occupied, which is the square root of the transition rate w. Thus

$$\psi_f = \sum_{\ell'} \sum_{m'} |\phi^{m'}_{f\ell'}\rangle \langle\phi^{m'}_{f\ell'}|A\cdot r|\phi^{m}_{i\ell}\rangle \quad , \tag{10}$$

where the sums extend over all possible values of the angular momentum quantum numbers. The values of the matrix elements tell us which final state transitions are allowed; since we are considering only electric dipole-allowed transitions, this means $\Delta\ell = \pm 1$ and we need only consider final states of $s(\ell' = 0)$ or $d(\ell' = 2)$ symmetry. Therefore the sum will have at most six terms.

The wavefunctions of an atom can be separated into radial and

angular parts:

$$|\phi^{m'}_{f\ell'}\rangle = R_{f\ell'}(r)\, Y_{\ell'm'}(\theta,\phi), \quad \text{and} \quad |\phi^{m}_{i\ell}\rangle = R_{i\ell}(r)\, Y_{\ell m}(\theta,\phi), \tag{11}$$

and the dot product $\underset{\sim}{A}\cdot\underset{\sim}{r}$ can be similarly broken down:

$$\underset{\sim}{A}\cdot\underset{\sim}{r} = A_x r\sin\theta\cos\phi + A_y r\sin\theta\sin\phi + A_z r\cos\theta\,. \tag{12}$$

The radial and angular integrals are separable,

$$\langle\phi^{m'}_{f\ell'}|\,\underset{\sim}{A}\cdot\underset{\sim}{r}\,|\phi^{m}_{i\ell}\rangle = \langle R_{f\ell'}|r|R_{i\ell}\rangle\cdot\langle Y_{\ell'm'}\left|\begin{array}{l} A_x\sin\theta\cos\phi \\ +A_y\sin\theta\sin\phi \\ +A_z\cos\theta \end{array}\right| Y_{\ell m}\rangle\,, \tag{13}$$

so that the electron intensity measured at the detector is

$$|\psi_f|^2 = \left|\sum_{\ell'}\left(\text{radial integral }(\ell')\right)\cdot\sum_{m'}\left(\text{angular integral }(\ell',m')\right)\cdot\phi^{m'}_{f\ell'}\right|^2 . \tag{14}$$

Note that the radial integrals are independent of the angular momentum substate; for a transition from a p state to a d state thus means all 5d states will have the same radial weighing factor. The angular integrals are calculated analytically; expressions of the form $\langle Y_{\ell'm'}|\sin\theta\cos\phi|Y_{\ell m}\rangle$ can be reduced to Clebsch-Gordan coefficients. The coefficients are zero for certain non-allowed transitions, such as $p_0 \rightarrow d_{\pm 2}$; it is here that the m' values are important.

THE PROGRAMS

Two programs are used to solve for the final detector intensity as in Eq. (14). A radial program calculates two radial integrals, one for s final states and one for d final states. Then an angle program uses these integrals as input, calculates the final detector intensity for the specified polarization, initial state, final state energy, and detector locations, and plots the specified intensity-versus-angle plots. These two types of programs are discussed separately.

1. Radial Programs.

These programs calculate the integrals

$$\int_0^\infty R_{f\ell'} \cdot r \cdot R_{i\ell} \cdot r^2 dr$$

where R represents the radial part of the corresponding initial or final state. We need expressions for the initial state and the final state, which are quite different since the first is a bound state of negative energy and the second is an outgoing electron wave of positive kinetic energy.

The initial state has been calculated for many different atoms by E. Clementi using self-consistent field methods. A linear combination of Slater orbitals of the form

$$\phi_i = C\, r^{n-1}\, e^{-xr}$$

was used, where the coefficients C and the exponents x were optimized to produce the minimum energy. The exact form of C is given in Reference 14 and is different for 2p and 3p orbitals. The orbitals are given as a

linear combination of four basis orbitals in the first case and eight in the second; these modifications necessitate slightly different programs for first row and second row atoms.

The final state is quite different. It must be calculated numerically as a solution to the radial Schroedinger equation. This is possible only because the final state energy is positive and a continuum of final states is available. The radial Schroedinger equation is

$$-\frac{1}{2}\frac{d^2}{dr^2} + \frac{\ell(\ell+1)}{2r^2} + V\,\phi = E\phi.$$

By transforming this equation into two first order differential equations, we can use existing computer integration routines to give us the value of Φ for any r. For program input we need the final state energy E, which is arbitrary; the potential V, which can be interpolated from a table of atomic potentials (we used values from Ref. 15); and the value and slope of the wavefunction at any one point. The last quantities are calculated as in Ref. 16.

Thus, a table of values of the final state wavefunction versus radial distance r, and an analytical expression for the initial state can be obtained. The integral can then be approximated as

$$\left[\sum_{j=1}^{n} \phi_f(r_j)\cdot\phi_i(r_j)\cdot r_j^3\right]\cdot\Delta r$$

where Δr is the distance between successive values of r, and the sum goes to an arbitrarily chosen cut-off point, after which any further contribution to the integral is neglected.

Since the values of the final wavefunction depend on the angular momentum ℓ, that entire calculation is performed twice, once for $\ell = 0$ and once for $\ell = 2$. The first number is called RADINT(1) and the second RADINT(2). The radial program will repeat the calculation for any number of energies; the output is a deck of cards each of which contains the energy, RADINT(1), and RADINT(2). These cards are then ready to be fed into the angular program where they form a table from which the radial integrals at any energy can be interpolated. Thus, one needs to run the radial programs only once for any one atom; the angular program can run at any number of intermediate energies on the same input cards.

2. Angular Programs

These programs calculate the detector intensity at specified angles using Eq. (14). The radial integrals used are the ones calculated and punched onto cards by the radial programs. The final states $\phi_f^{m'}$, are Coulomb waves, the angular dependence of which is described by the spherical harmonics and the radial dependence of which is set equal to one since it does not affect the detector intensity. Thus, the program calculates

$$\left[\sum_{\ell=1,2} \text{RADINT}(\ell) \sum_{m'} \left(\langle Y_{\ell' m'} | A_x \sin\theta\cos\phi | Y_{\ell m} \rangle + \langle Y_{\ell' m'} | A_y \sin\theta\sin\phi | Y_{\ell m} \right.\right.$$
$$\left.\left. + \langle Y_{\ell' m'} | A_z \cos\theta | Y_{\ell m} \rangle \right) \cdot Y_{\ell' m'}(\theta,\phi) \right] ,$$

where the values of RADINT(ℓ), ℓ, m, A_x, A_y, and A_z are specified as input. The three angular integrals reduce to simple numbers multiplied by the components of A. The program calculates all the integrals and multiplies

by RADINT(1) or RADINT(2), as appropriate, to obtain a set of coefficients which depend on the final state parameters ℓ' and m'. Then it cycles through a series of angle loops wherein it calculates the values of the six spherical harmonics $Y_{\ell'm'}$ at the specified angle, multiplies by the proper coefficient, and sums and squares these numbers. Note that the angular integrals and all quantities derived from them are complex numbers; the last operation is actually taking the square of the magnitude of $\psi_f(\theta,\phi)$ so as to produce a real number.

After finishing the angle loops, the program has three arrays: two contain angle values, and the third contains the detector currents at these angles. Plotting sequences normalize all distributions to a maximum value of unity and give a two-dimensional plot of current as a function of one angle at a fixed value of the other angle.

DATA

The radial programs were run for six atoms: C, N, O, Si, P, and S. The values of the overlap integrals and their ratios are shown in Tables 1 and 2. The first column in these tables is the kinetic energy in eV of the outgoing electron (ENG); the second column is the radial overlap integral for the s final state (RAD1); the third column is the overlap integral for the d final state (RAD2); and the last column is the ratio of the d integral to the s integral (RAD3), with the last three columns expressed in scientific notation. Only the first four digits are significant. The values of the radial integrals and their ratios as a function of energy are plotted in Figs. 1 and 2. Fig. 1 shows the values for carbon, nitrogen, and oxygen for energies from zero to 100 eV. The first row of plots is the overlap integral for the final state s-wave, the second row is for the d-wave, and the third is the ratio of d-wave to s-wave integrals. Note that the ordinates have different scales, with the d-wave values being up to eight times the s-wave values. There are no units shown because only the relative values are important.

Fig. 2 is essentially the same as Fig. 1, plotting the radial integrals and their ratios as a function of energy for the second-row atoms. Note that here the horizontal axis is not at zero for the first and third rows, since there are also negative values of the integrals here. In all cases the integrals converge to zero at high energies, which is reasonable since at high energies the final states oscillate very rapidly, causing the positive and negative parts of the integral to cancel. The reason these integrals can be negative where the integrals

for the first row atoms are always positive is that the radial part of the 3p orbital is negative near the nucleus and positive later, whereas that of the 2p orbital has no radial node.

Figs. 3 and 4 show the values of the one initial and two final state wave functions for oxygen and sulfur at 10 eV, and the products $\psi_i \cdot \psi_f \cdot r$, which are the radial integrands. The horizontal axis is radial distance from the nucleus, given in atomic units (0.529 Å). The functions were calculated and integrated to 10 Bohr for first row atoms and to 15 Bohr for second row atoms, since the remainder of space contributes little to the integral. The vertical axis shows the relative magnitudes of the three wave functions and the relative values of the two integrands. Note the shapes of the initial state wavefunctions for the two cases. The signs of the initial states are unimportant since all values are eventually squared, but the fact that the s and d wavefunctions can overlap the initial state with opposite signs in Fig. 4 is important. Where that is the case, the outgoing waves add with opposite phase, the difference being that between $\psi_s + \psi_d$ and $\psi_s - \psi_d$. This effect will become clearer in the discussion of angular plots.

Another important feature of the radial plots is that due to the sign change in the d-wave overlap integral, there is a point where the ratio of d- to s-wave integrals is zero. At this point, the outgoing electron is exclusively s-wave in character. This is an important point since the emission should be spherically symmetric at this energy. It should thus be possible to separate emissions from two initial states of different symmetries if one has this property since all angular dependences will then be due to electrons from the other.

The angular plots emphasize these points. For each atom, I have plotted the polar and azimuthal angle dependences for photoemission from a p_z orbital using x-polarized, z-polarized, and xz-unpolarized light. These plots are shown in Figs. 5-10 for all six atoms at an arbitrarily chosen energy of 10.0 eV. The top plots are the polar angle dependences in the xz-plane. The bottom plots show the azimuthal angle dependence in the xy-plane. These plots are at a constant polar angle of 10 degrees. Note that the unpolarized light produces a distribution similar to the z-polarized light; this is because the emission is much stronger for z-polarized than x-polarized light. The only difference between the atoms in these plots is the values of the radial integrals which were input into the program. Thus, the z-polarized light emission from carbon (Fig. 5), which has a higher d-to-s ratio that oxygen (Fig. 7), looks more like a d_{z^2} orbital than does that from oxygen. What happens is that the outgoing s-wave adds to the appropriate combination of d-waves (which is only d_{z^2} for this combination of initial state and polarization) before squaring, which means that phase factors are important. For positive values of the d-to-s ratio, the larger is the proportion of s-wave, and the smaller is the small lobe on this plot compared to the large lobe. This trend can be seen in the C–N–O series (Figs. 5,6, and 7).

If the d-to-s ratio is negative, however, the s-wave will add constructively to the small lobe and destructively to the large lobe. Thus, the appearance of photoemission from Si, P, and S (Figs. 8, 9, and 10) for this polarization is very different from the first row atoms. Emission is a minimum at small polar angles, whereas it is a maximum in the other case (Figs. 5-7). This trend would be expected to change at

different energies since the radial integral ratio changes from negative to positive.

Figs. 11 and 12 show the shapes of the z-polarized light distributions for oxygen and sulfur, respectively, at various energies. Note that the oxygen distributions retain the same shape for all energies but the sulfur plots change dramatically, looking more like the oxygen plots at higher energies where the d-to-s ratio reaches its largest positive value.

It is thus apparent that within the approximations used, the shape of the angular distribution of photoelectrons depends on three factors: the atom (and orbital) from which the electron is emitted, the energy with which it leaves, and the polarization of the exciting radiation. The first two factors determine the ratio of d-wave to s-wave phases and intensities in the final state and the third determines which d-waves will be used. This treatment is a useful starting point for calculation of photoelectron distributions expected from chemisorption systems.

SUGGESTIONS FOR FUTURE WORK

Two types of extensions to this work would be valuable. One is to add the capability to treat molecules, and the other is to consider substrate multiple scattering effects in a LEED-type final state. The second is perhaps more straightforward as our research group has possession of programs written for this purpose by Michel Van Hove and S. Y. Tong. The programs are long and complicated and appear to suffer from convergence problems. If they can be fixed to run properly, it should be straightforward to adapt them to our uses.

Treating molecules will be more difficult. One must have an analytic or numerical expression for the initial state and must be able to compensate for the reduced symmetry of a molecule over an atom. In other words, the final state for CO will no longer be a sum of six spherical harmonics. It is suggested that future workers either examine the scattered-wave-$X\alpha$-approach of Davenport[2] and of Johnson[17] or the Green's-function approach of Gadzuk.[3,4,5] In the latter case, some further data will be needed to pinpoint the extent of orbital mixing before valuable comparisons with experiment can be made.

REFERENCES

1. Eastman, D. E. and Nathan, M. I., Physics Today (April 1975) 44-51.
2. Davenport, J., Phys. Rev. Lett. 36 (1976) 945-949.
3. Gadzuk, J. W., Surf. Sci. 53 (1975) 132-143.
4. Gadzuk, J. W., Solid State Commun. 15 (1974) 1011-1016.
5. Gadzuk, J. W., Phys. Rev. B. 10 (1976) 5030-5044.
6. Gadzuk, J. W., Phys. Rev. B. 12 (1975) 5608-5614.
7. Jacobi, K., Scheffler, M., Kambe, K., and Forstmann, F., Solid State Commun. 22 (1977) 17-20.
8. Liebsch, A., Phys. Rev. Lett. 38 (1977) 248-251.
9. Liebsch, A., Phys. Rev. B. 13 (1976) 544-555.
10. Tong, S. Y., and Van Hove, M. A., Solid State Commun. 19 (1976) 543-546.
11. Scheffler, M., Kambe, K., and Forstmann, F., Solid State Commun. 25 (1978) 93-99.
12. Horn, K., Bradshaw, A. M., and Jacobi, K., Surf. Sci. 72 (1978) 719-732.
13. Schiff, L. I. Quantum Mechanics, 3rd ed., Sections 24, 37, and 44. McGraw-Hill (New York, 1968).
14. Clementi, E., IBM J. Res. and Devel. 9 (1965) 2-19 (Supplement).
15. Lu, C. C., Carlson, T. A., Malik, F. B., Tucker, T. C., and Nestor, C. W., Jr., Atomic Data 3 (1971) 1-31.
16. Pendry, J. B. Low Energy Electron Diffraction, Appendix C4, Academic (New York, 1974).
17. Johnson, K. H., J. Chem. Phys. 45 (1966) 3085-3095.

CARBON

ENG	RAD1	RAD2	RAD3
1.000000	0.26194E 00	0.19848E 01	0.75771E 01
5.000000	0.17526E 00	0.10168E 01	0.58019E 01
10.000000	0.12580E 00	0.53748E 00	0.42724E 01
15.000000	0.95002E-01	0.32121E 00	0.33810E 01
20.000000	0.71842E-01	0.20333E 00	0.28302E 01
25.000000	0.55990E-01	0.13540E 00	0.24183E 01
30.000000	0.46163E-01	0.95252E-01	0.20634E 01
35.000000	0.39644E-01	0.69913E-01	0.17635E 01
40.000000	0.34202E-01	0.52420E-01	0.15326E 01
45.000000	0.28978E-01	0.39645E-01	0.13681E 01
50.000000	0.24158E-01	0.30317E-01	0.12549E 01
55.000000	0.20233E-01	0.23699E-01	0.11713E 01
60.000000	0.17449E-01	0.19085E-01	0.10938E 01
65.000000	0.15655E-01	0.15789E-01	0.10085E 01
70.000000	0.14445E-01	0.13254E-01	0.91758E 00
75.000000	0.13389E-01	0.11142E-01	0.83216E 00
80.000000	0.12213E-01	0.93107E-02	0.76235E 00
85.000000	0.10857E-01	0.77452E-02	0.71341E 00
90.000000	0.94292E-02	0.64707E-02	0.68624E 00
95.000000	0.81121E-02	0.54938E-02	0.67724E 00
100.000000	0.70621E-02	0.47813E-02	0.67704E 00

NITROGEN

ENG	RAD1	RAD2	RAD3
1.000000	0.19612E 00	0.11402E 01	0.58140E 01
5.000000	0.14447E 00	0.68457E 00	0.47385E 01
10.000000	0.10700E 00	0.40499E 00	0.37850E 01
15.000000	0.83012E-01	0.26047E 00	0.31378E 01
20.000000	0.66196E-01	0.17688E 00	0.26721E 01
25.000000	0.54199E-01	0.12528E 00	0.23115E 01
30.000000	0.45496E-01	0.91953E-01	0.20211E 01
35.000000	0.38885E-01	0.69454E-01	0.17861E 01
40.000000	0.33556E-01	0.53618E-01	0.15978E 01
45.000000	0.29102E-01	0.42095E-01	0.14465E 01
50.000000	0.25369E-01	0.33548E-01	0.13224E 01
55.000000	0.22296E-01	0.27133E-01	0.12170E 01
60.000000	0.19804E-01	0.22263E-01	0.11241E 01
65.000000	0.17776E-01	0.18504E-01	0.10409E 01
70.000000	0.16077E-01	0.15541E-01	0.96665E 00
75.000000	0.14592E-01	0.13156E-01	0.90158E 00
80.000000	0.13249E-01	0.11207E-01	0.84588E 00
85.000000	0.12018E-01	0.96018E-02	0.79897E 00
90.000000	0.10902E-01	0.82799E-02	0.75946E 00
95.000000	0.99167E-02	0.71930E-02	0.72534E 00
100.000000	0.90696E-02	0.62988E-02	0.69449E 00

OXYGEN

ENG	RAD1	RAD2	RAD3
1.000000	0.16029E 00	0.79974E 00	0.49894E 01
5.000000	0.12152E 00	0.50226E 00	0.41332E 01
10.000000	0.92756E-01	0.31332E 00	0.33779E 01
15.000000	0.73669E-01	0.21090E 00	0.28628E 01
20.000000	0.59984E-01	0.14890E 00	0.24824E 01
25.000000	0.50006E-01	0.10905E 00	0.21807E 01
30.000000	0.42562E-01	0.82337E-01	0.19345E 01
35.000000	0.36742E-01	0.63724E-01	0.17343E 01
40.000000	0.31969E-01	0.50271E-01	0.15725E 01
45.000000	0.27963E-01	0.40264E-01	0.14399E 01
50.000000	0.24610E-01	0.32689E-01	0.13283E 01
55.000000	0.21840E-01	0.26888E-01	0.12311E 01
60.000000	0.19567E-01	0.22394E-01	0.11445E 01
65.000000	0.17680E-01	0.18861E-01	0.10668E 01
70.000000	0.16067E-01	0.16033E-01	0.99788E 00
75.000000	0.14643E-01	0.13731E-01	0.93776E 00
80.000000	0.13356E-01	0.11833E-01	0.88595E 00
85.000000	0.12190E-01	0.10257E-01	0.84138E 00
90.000000	0.11145E-01	0.89438E-02	0.80249E 00
95.000000	0.10227E-01	0.78493E-02	0.76753E 00
100.000000	0.94339E-02	0.69343E-02	0.73504E 00

Table 1. Radial integrals (RAD1 and RAD2) and their ratio (RAD3) for carbon, nitrogen, and oxygen at different energies (ENG).

SILICON

ENG	RAD1	RAD2	RAD3
1.000000	-0.32160E 00	0.31110E 00	-0.96735E 00
5.000000	-0.19017E 00	0.89514E-01	-0.47072E 00
10.000000	-0.10977E 00	0.16705E-01	-0.15218E 00
15.000000	-0.74100E-01	-0.14027E-02	0.18930E-01
20.000000	-0.53039E-01	-0.66184E-02	0.12478E 00
25.000000	-0.39560E-01	-0.74054E-02	0.18719E 00
30.000000	-0.31962E-01	-0.69903E-02	0.21871E 00
35.000000	-0.26434E-01	-0.64760E-02	0.24499E 00
40.000000	-0.21406E-01	-0.57899E-02	0.27048E 00
45.000000	-0.17602E-01	-0.49990E-02	0.28400E 00
50.000000	-0.15270E-01	-0.43428E-02	0.28440E 00
55.000000	-0.13565E-01	-0.38651E-02	0.28494E 00
60.000000	-0.11757E-01	-0.34444E-02	0.29296E 00
65.000000	-0.99228E-02	-0.30131E-02	0.30365E 00
70.000000	-0.85122E-02	-0.26145E-02	0.30714E 00
75.000000	-0.76866E-02	-0.23072E-02	0.30016E 00
80.000000	-0.71766E-02	-0.20876E-02	0.29090E 00
85.000000	-0.66171E-02	-0.19050E-02	0.28788E 00
90.000000	-0.58813E-02	-0.17190E-02	0.29228E 00
95.000000	-0.51182E-02	-0.15302E-02	0.29897E 00
100.000000	-0.45501E-02	-0.13646E-02	0.29990E 00

PHOSPHORUS

ENG	RAD1	RAD2	RAD3
1.000000	-0.25557E 00	0.17240E 00	-0.67455E 00
5.000000	-0.17344E 00	0.64822E-01	-0.37373E 00
10.000000	-0.11147E 00	0.17901E-01	-0.16060E 00
15.000000	-0.78614E-01	0.23947E-02	-0.30461E-01
20.000000	-0.57606E-01	-0.31751E-02	0.55116E-01
25.000000	-0.44023E-01	-0.48284E-02	0.10968E 00
30.000000	-0.35596E-01	-0.51320E-02	0.14417E 00
35.000000	-0.29333E-01	-0.50205E-02	0.17115E 00
40.000000	-0.24180E-01	-0.46565E-02	0.19258E 00
45.000000	-0.20378E-01	-0.41840E-02	0.20532E 00
50.000000	-0.17763E-01	-0.37594E-02	0.21164E 00
55.000000	-0.15662E-01	-0.34087E-02	0.21764E 00
60.000000	-0.13663E-01	-0.30795E-02	0.22539E 00
65.000000	-0.11857E-01	-0.27514E-02	0.23204E 00
70.000000	-0.10475E-01	-0.24531E-02	0.23418E 00
75.000000	-0.95170E-02	-0.22116E-02	0.23238E 00
80.000000	-0.87595E-02	-0.20194E-02	0.23054E 00
85.000000	-0.79896E-02	-0.18490E-02	0.23143E 00
90.000000	-0.71724E-02	-0.16822E-02	0.23453E 00
95.000000	-0.64211E-02	-0.15222E-02	0.23706E 00
100.000000	-0.58531E-02	-0.13827E-02	0.23624E 00

SULFUR

ENG	RAD1	RAD2	RAD3
1.000000	-0.22142E 00	0.11008E 00	-0.49713E 00
5.000000	-0.15230E 00	0.44849E-01	-0.29448E 00
10.000000	-0.10206E 00	0.14457E-01	-0.14165E 00
15.000000	-0.73222E-01	0.31767E-02	-0.43385E-01
20.000000	-0.54838E-01	-0.12614E-02	0.23003E-01
25.000000	-0.42851E-01	-0.29120E-02	0.67955E-01
30.000000	-0.34875E-01	-0.34562E-02	0.99103E-01
35.000000	-0.29003E-01	-0.35533E-02	0.12252E 00
40.000000	-0.24457E-01	-0.34265E-02	0.14010E 00
45.000000	-0.21044E-01	-0.32037E-02	0.15224E 00
50.000000	-0.18469E-01	-0.29701E-02	0.16081E 00
55.000000	-0.16350E-01	-0.27489E-02	0.16812E 00
60.000000	-0.14480E-01	-0.25314E-02	0.17482E 00
65.000000	-0.12867E-01	-0.23169E-02	0.18007E 00
70.000000	-0.11561E-01	-0.21179E-02	0.18319E 00
75.000000	-0.10522E-01	-0.19442E-02	0.18477E 00
80.000000	-0.96376E-02	-0.17933E-02	0.18607E 00
85.000000	-0.88161E-02	-0.16561E-02	0.18785E 00
90.000000	-0.80406E-02	-0.15266E-02	0.18986E 00
95.000000	-0.73480E-02	-0.14054E-02	0.19127E 00
100.000000	-0.67723E-02	-0.12968E-02	0.19148E 00

Table 2. Radial integrals for silicon, phosphorus, and sulfur, as in Fig. 1.

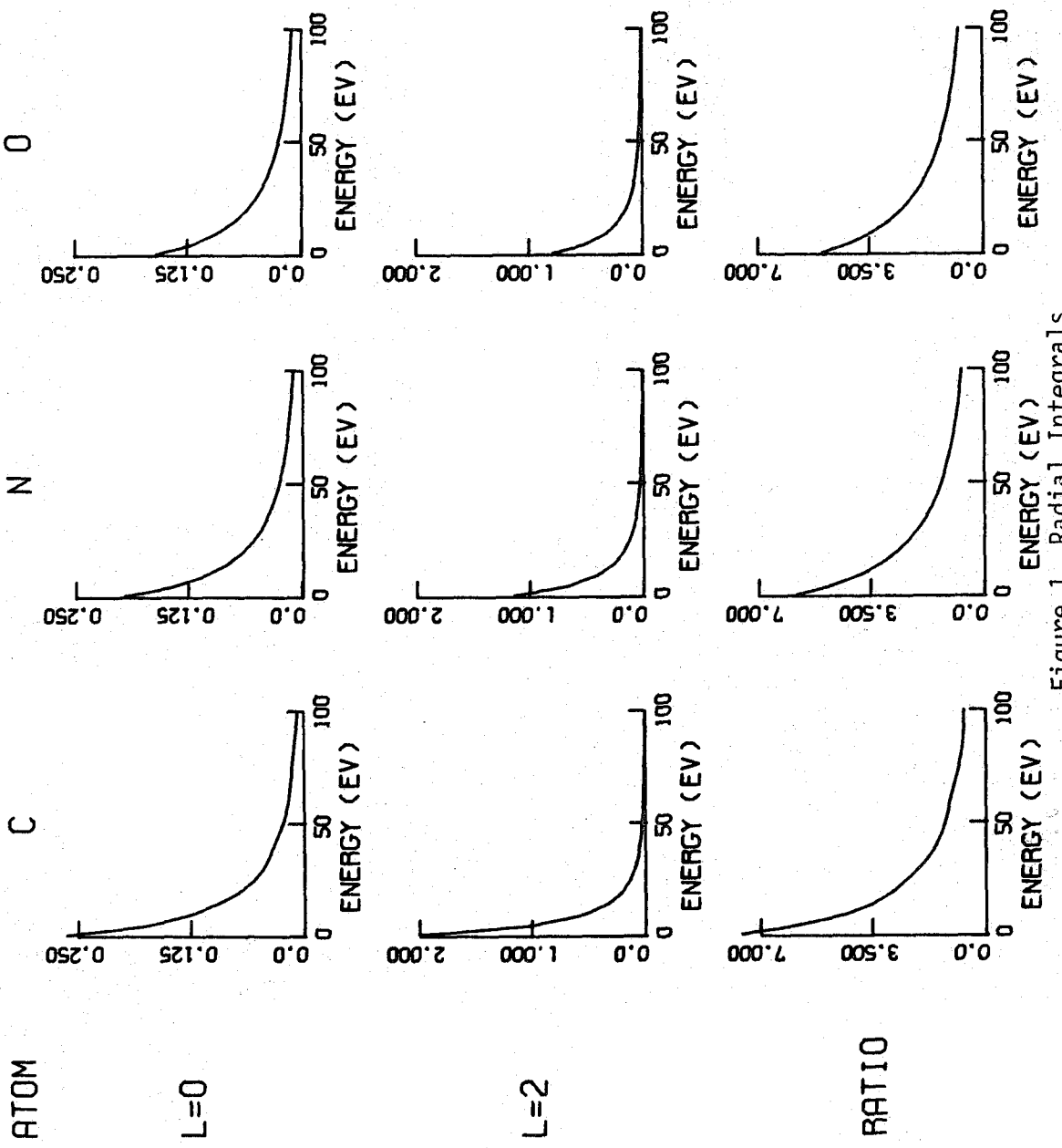

Figure 1. Radial Integrals

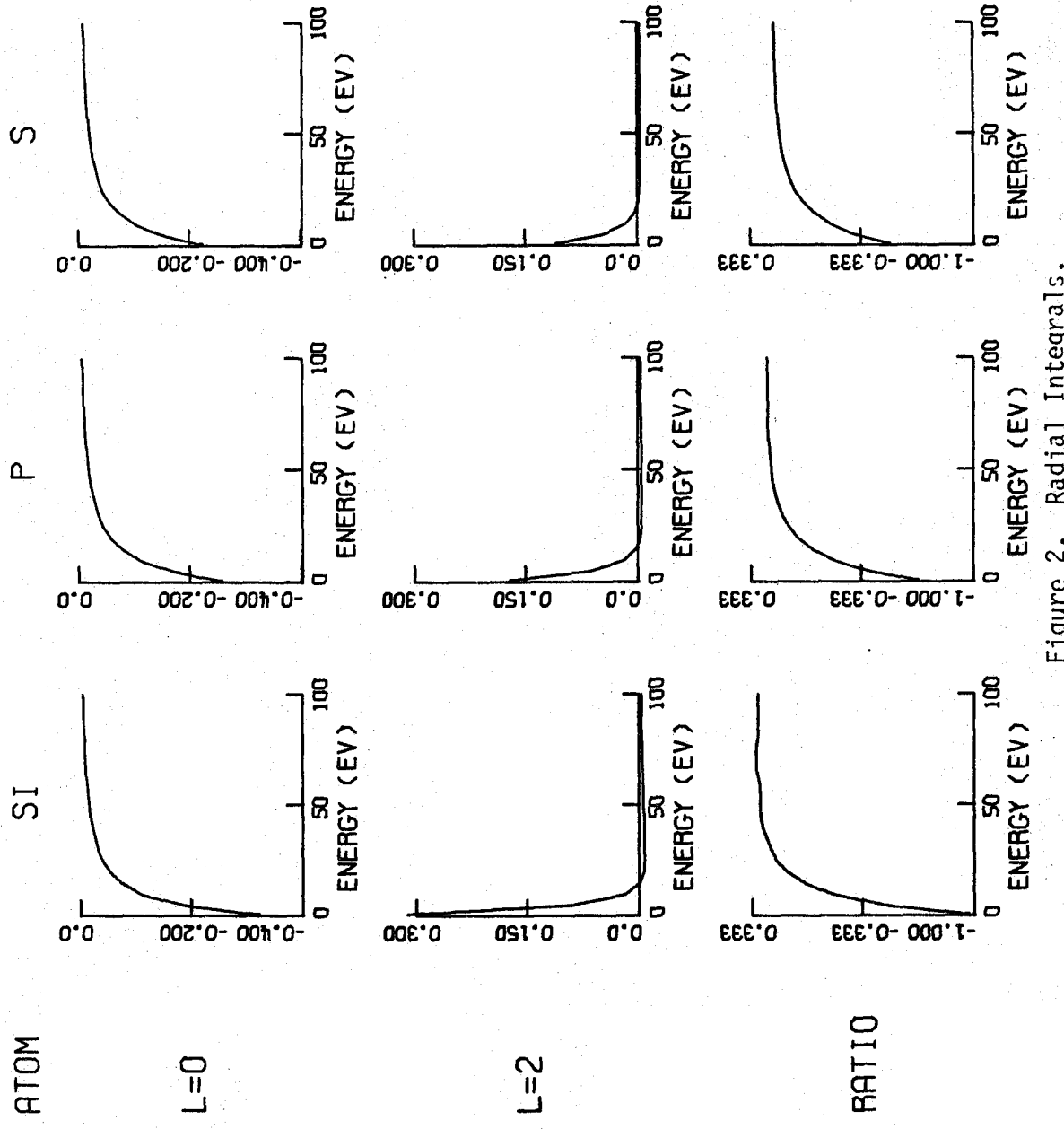

Figure 2. Radial Integrals.

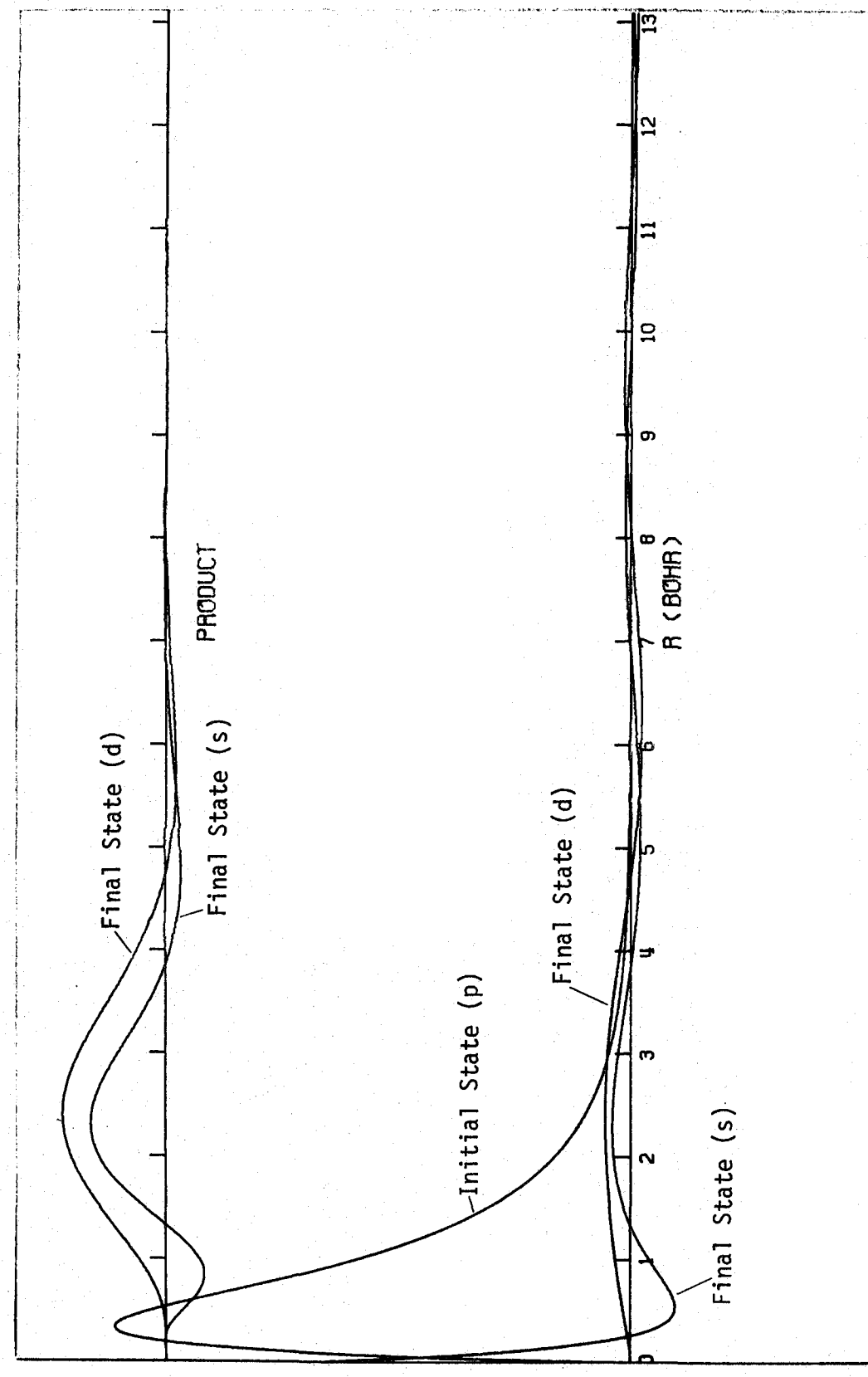

Figure 3. Oxygen wavefunctions and products $\psi_i \cdot \psi_f \cdot r$. Final state energy is 10.0 eV.

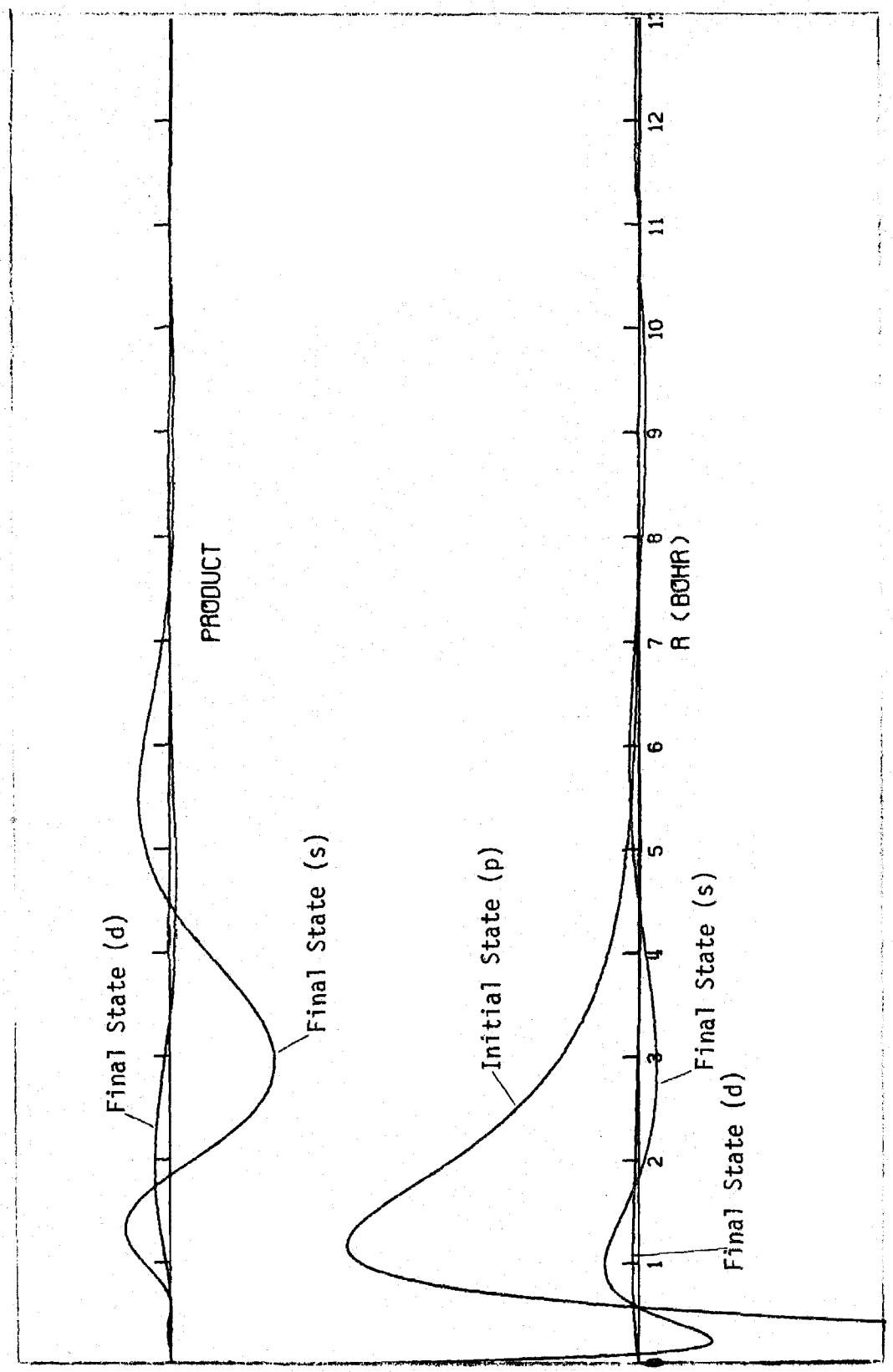

Figure 4. Sulfur wavefunctions and products $\psi_i \cdot \psi_f \cdot r$.
Final state energy is 10.0 eV.

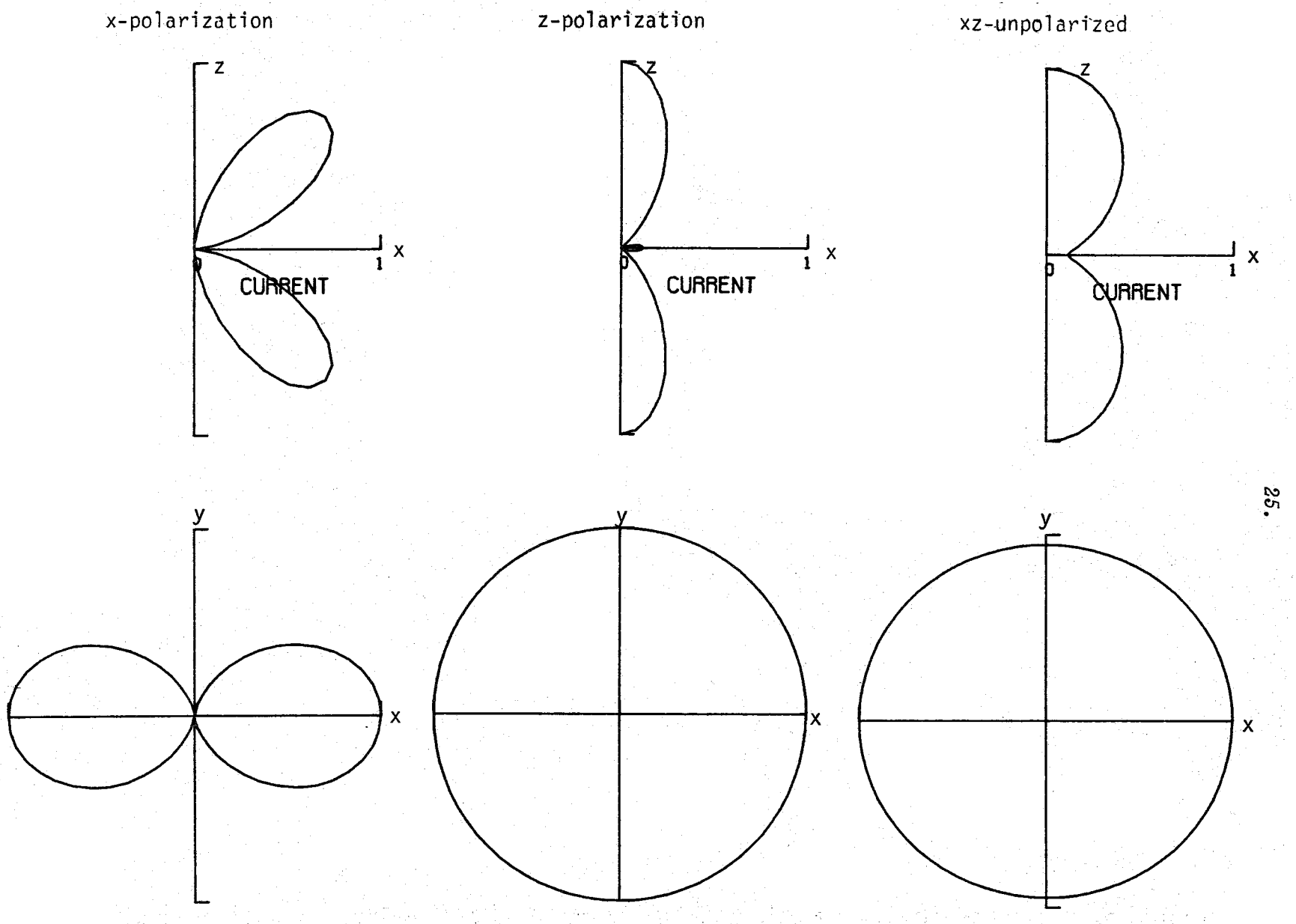

Figure 5. Carbon photoemission patterns from a $2p_z$ orbital; final state energy is 10.0 eV.

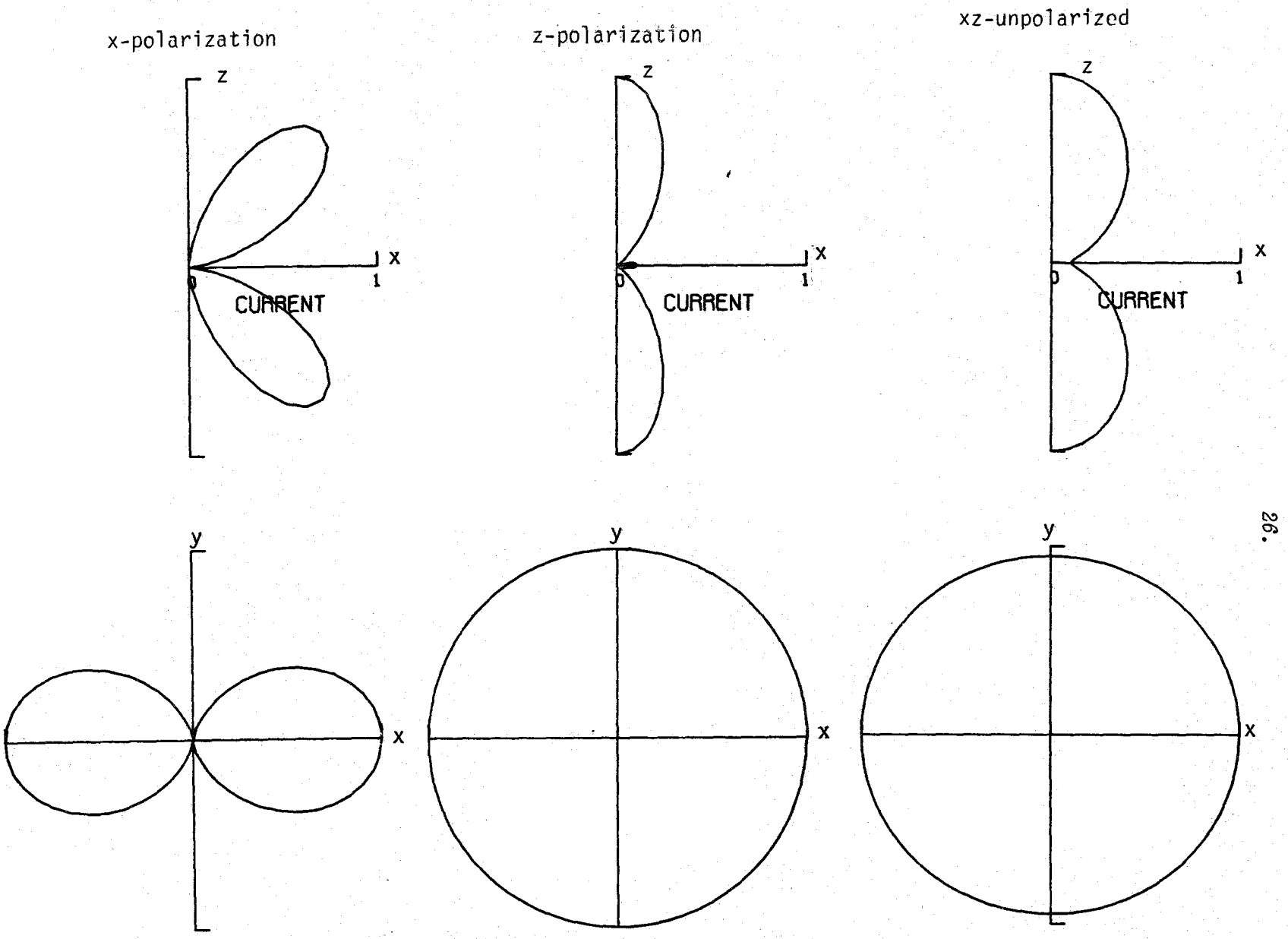

Figure 6. Nitrogen photoemission patterns from a $2p_z$ orbital; final state energy is 10.0 eV.

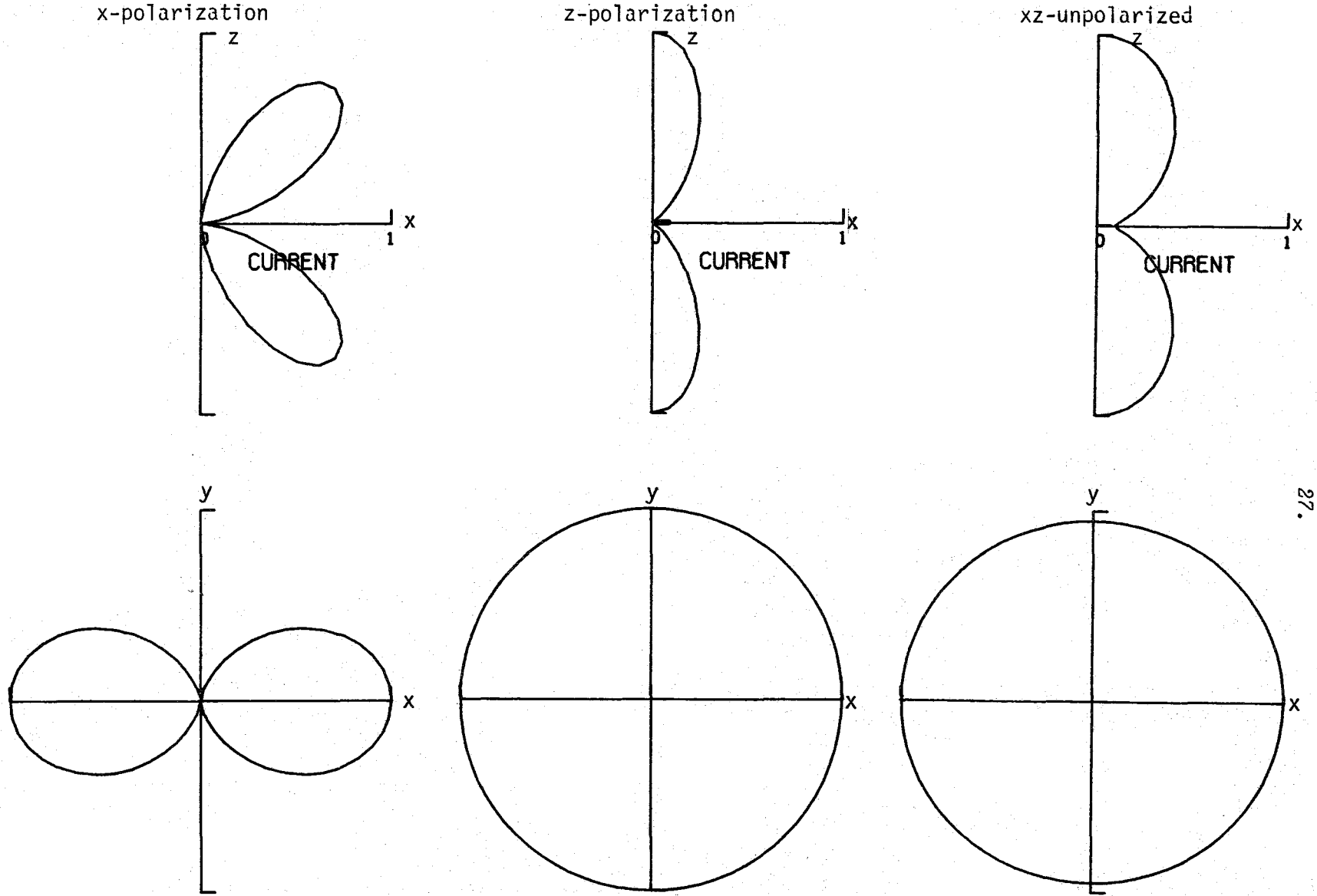

Figure 7. Oxygen photoemission patterns from a $2p_z$ orbital; final state energy is 10.0 eV.

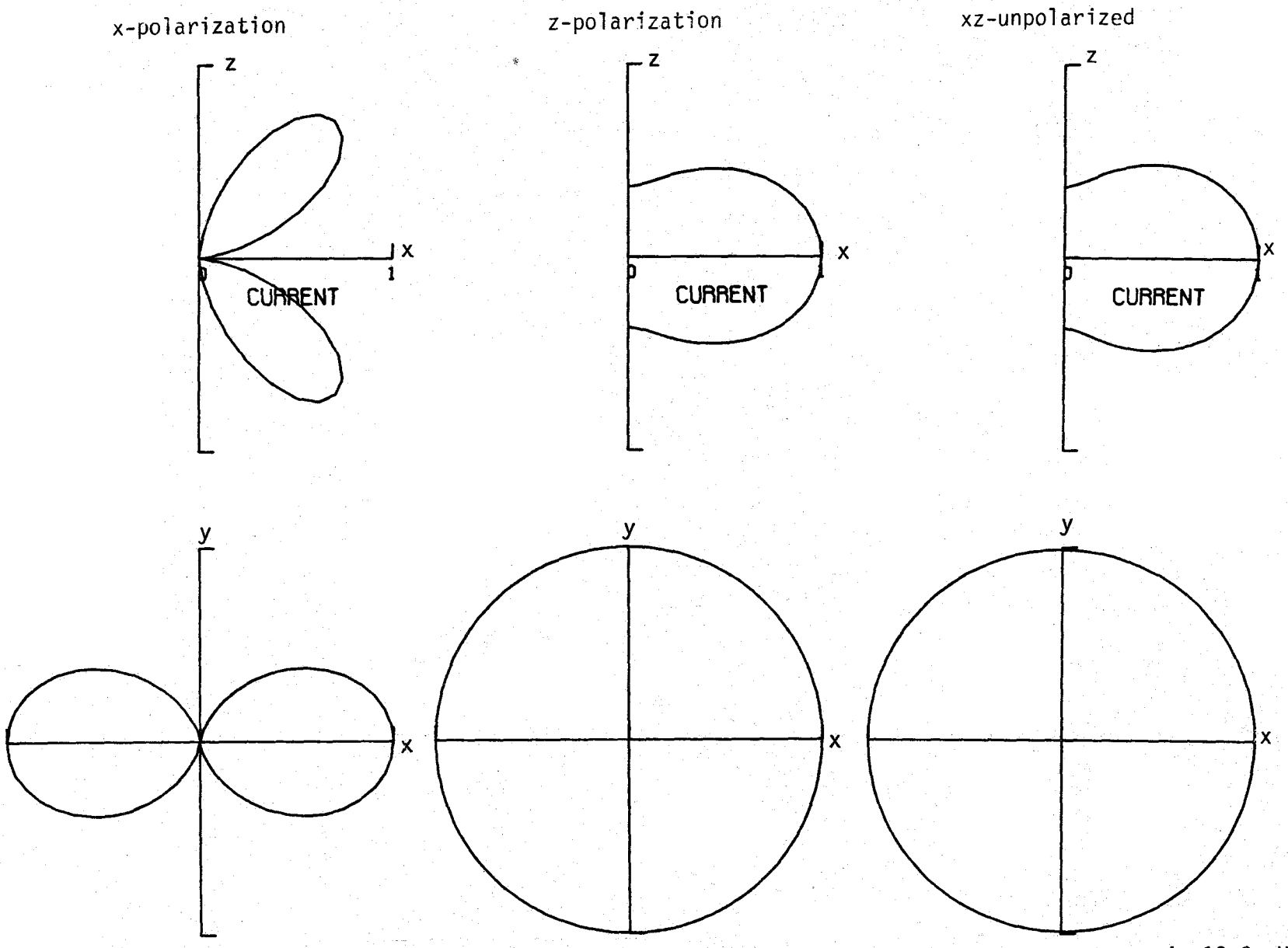

Figure 8. Silicon photoemission patterns from a $3p_z$ orbital; final state energy is 10.0 eV.

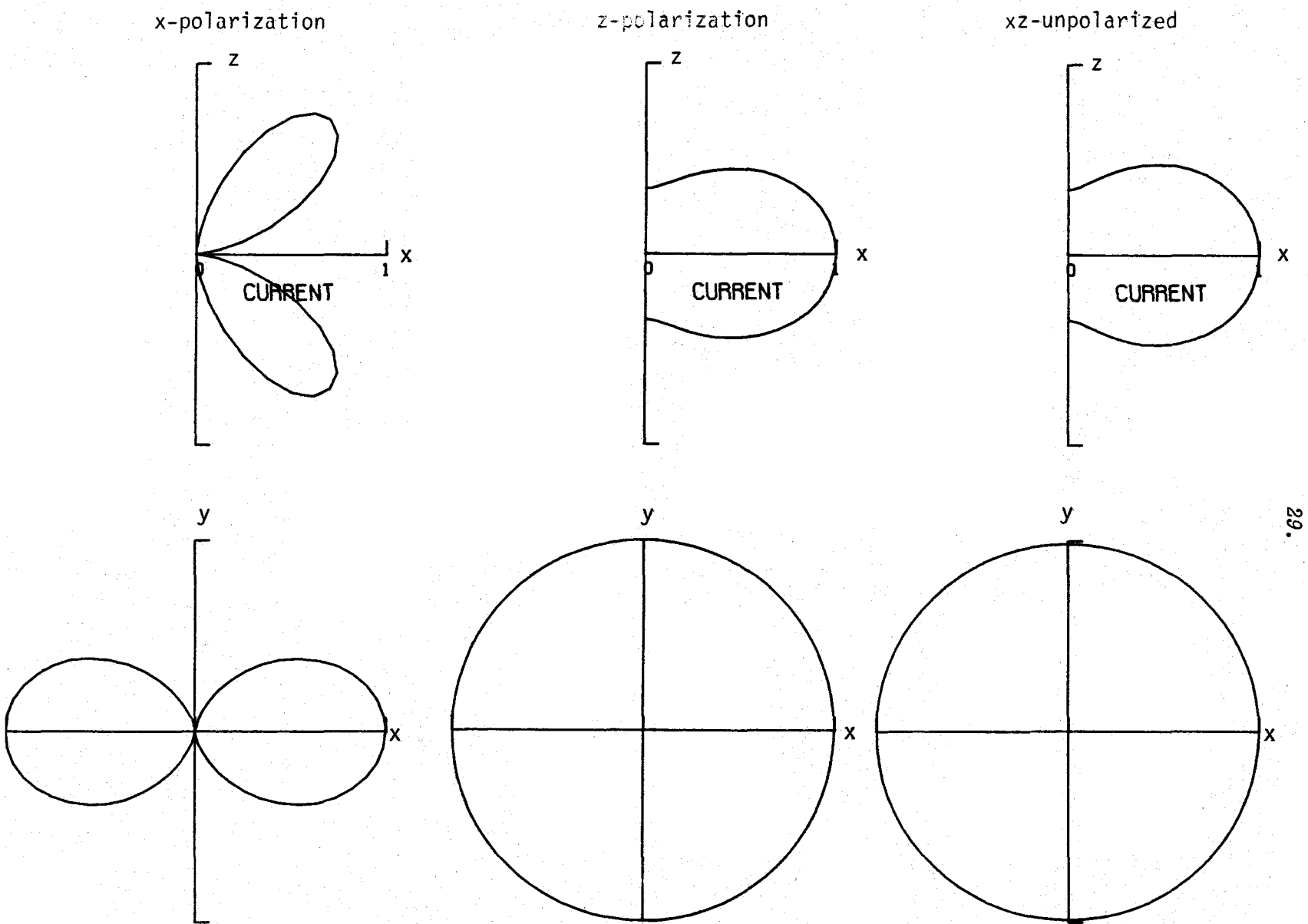

Figure 9. Phosphorous photoemission patterns from a $3p_z$ orbital; final state energy is 10.0 eV.

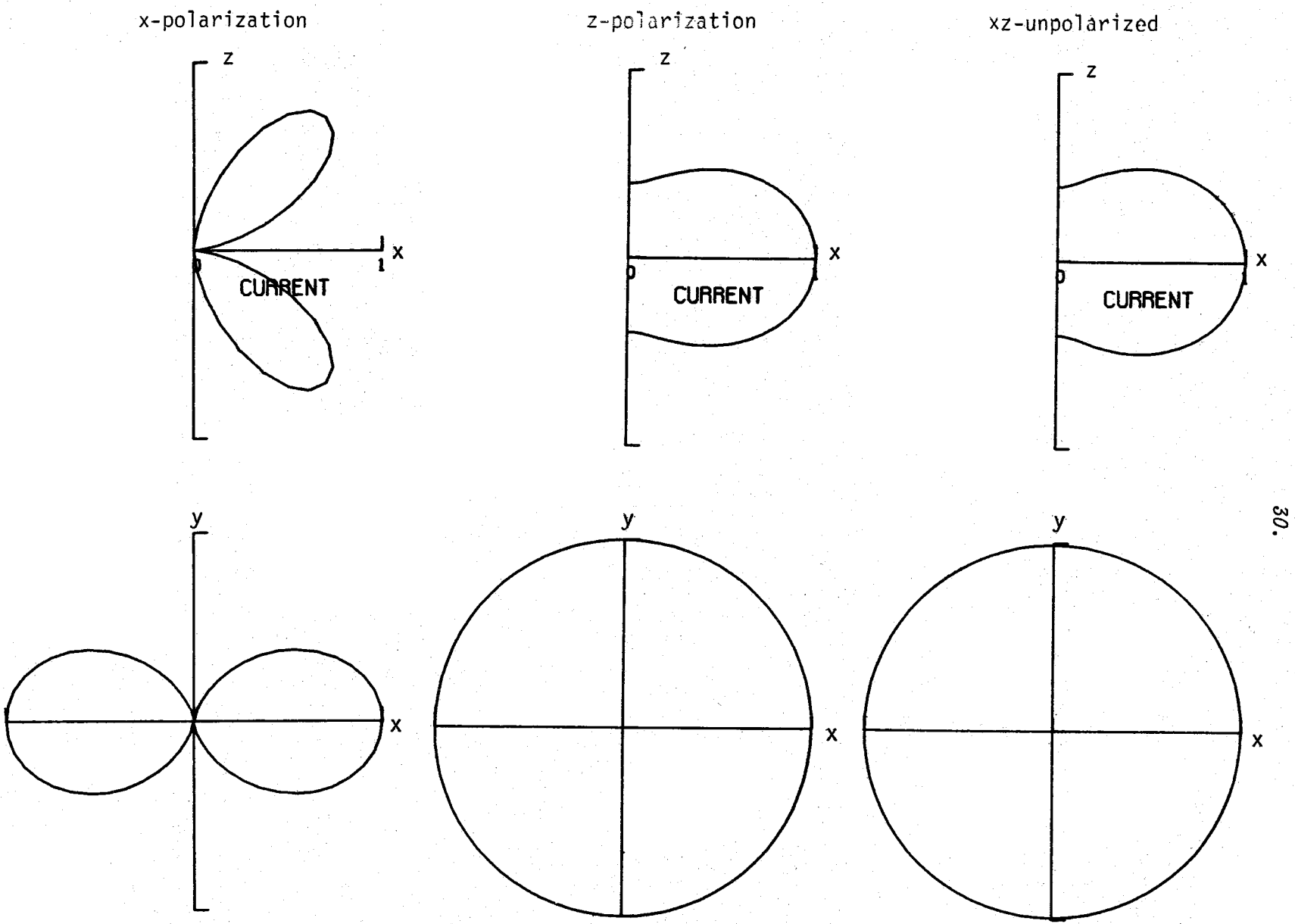

Figure 10. Sulfur photoemission patterns from a $3p_z$ orbital; final state energy is 10.0 eV.

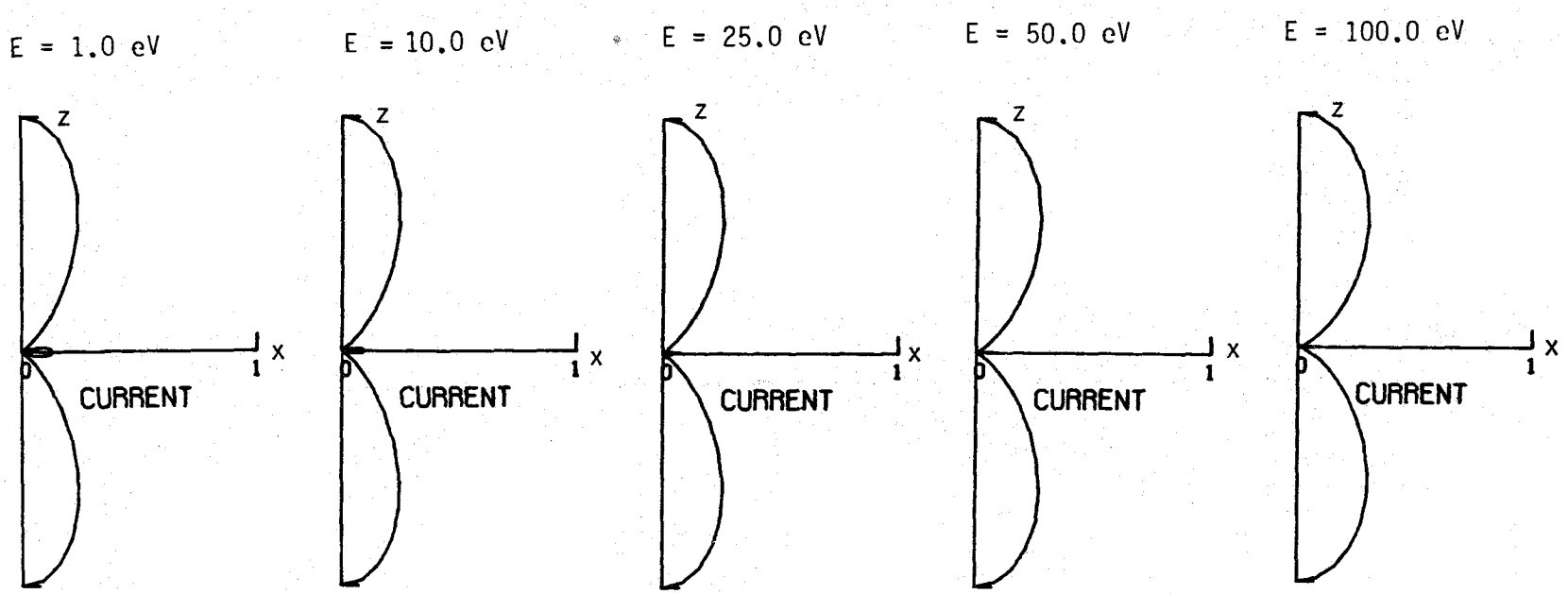

Figure 11. Oxygen photoemission patterns for z-polarized light.

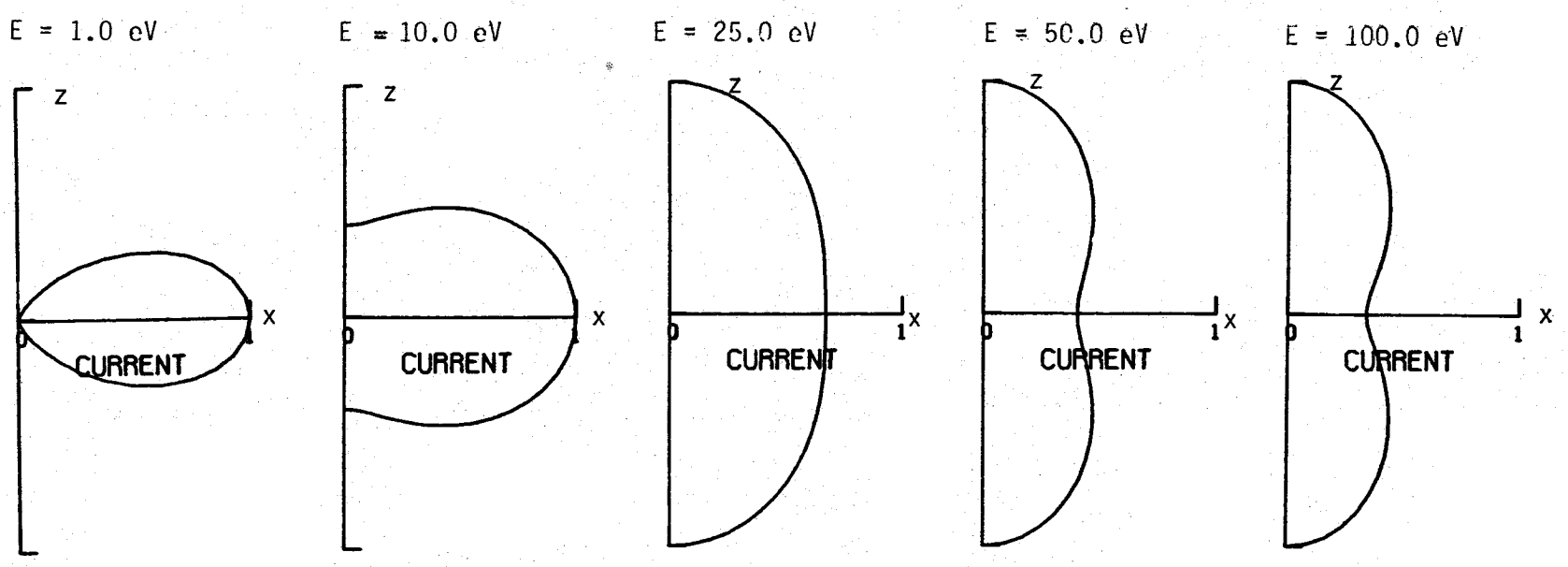

Figure 12. Sulfur photoemission patterns for z-polarized light.

APPENDIX 1

Angle-Resolved Photoemission Programs

The four programs which follow are of three types: radial programs (RADOXYG, RADSULF), an angular program (ANGSULF), and a tabulation and plot program (RADTABL). The first two are to be used for first-row and second-row atoms, respectively, as the manner of calculating the initial state differs in the two cases. The third program can be used for all atoms and requires as input the radial integrals which are calculated and punched onto cards in the radial programs. This version assumes one uses radial integrals at an energy for which there are integrals calculated; alternately, one could call the subroutine RADIAL to interpolate from a table. In this case, the table should be read into the variables ENERGY, SDUM, and KDUM, which are already dimensioned. Plots from this program are shown in Fig. 10; the same program with different input data plotted Figs. 5 through 12.

The last program collects the radial integral values calculated in the radial programs for up to eight atoms. It calculates the ratio of the d-wave final state integral to the s-wave final state integral for each atom and energy, lists the values in a table, and plots the integrals and their ratios as a function of energy. This program plotted Figs. 1 and 2 and printed Tables 1 and 2. The data is not shown since it consists mainly of the output cards from the radial programs.

Program 1.

```
//RADOXYG JOB (9805Z,WHW,CHE),SHEARD,TIME=(1,50)
/*JOBPARM IOC=15
//       EXEC  FORTG
//SYSPLTDN DD SYSOUT=(N,,GSW4)
//FORT   DD    *
C       4.   INITIAL STATE, GIVEN AS A LINEAR COMBINATION OF SLATER ORBITALS.
C            THIS PROGRAM IS FOR 2P ORBITALS, USING 4 TOTAL ORBITALS AS
      REAL LPLUS1
      DIMENSION RADINT(2)
      DIMENSION RR(150),VV(150),Y(2),DY(2)
      DIMENSION YPT(800),SUM1(800),SUM2(800)
      DIMENSION DD(3)
      DIMENSION XPLT(800),YPLT(800),PHINIT(800),ACOEF(4),AEXP(4)
      COMMON F, LPLUS1, Z, L
      COMMON/VAL/RR,VV,NPOT
      EXTERNAL DERIV
      DATA DD/0.,0.,0./
  401 FORMAT (2X,2F15.8)
  499 FORMAT(3X,'OXYGEN 2P')
  500 FORMAT (2F15.8)
  501 FORMAT (I3)
  502 FORMAT (F7.4)
  503 FORMAT(' ATOMIC NUMBER =',F4.1)
  504 FORMAT (50X,'L =',I3,'     NUM =',I4)
  507 FORMAT (' ENERGY(EV)',11X,'RADINT:  L=0',14X,'L=2')
  508 FORMAT(F15.7,15X,E15.7,2X,E15.7,30X,7HTNORM =,E15.7)
  509 FORMAT (3E15.8)
  530 FORMAT ( 1X,'R=',F18.7,'Y(1)=',E15.7,'DY(1)=',E14.7)
  540 FORMAT ( 21X,'Y(2)=',E15.7,'DY(2)=',E14.7)
  550 FORMAT ( 'ERROR OCCURRED, K=-1, DID NOT CONVERGE')
      N=2
      RSTART=0.003
      C=1.0
      RMAX=15.0
      DR=0.02
      EPS=0.0
      WRITE (6,499)
      WRITE (7,499)
      READ(5,502) Z
      WRITE(6,503)  Z
      READ (5,501) NPOT
      WRITE(6,501) NPOT
      READ (5,500) ((RR(I),VV(I)),I=1,NPOT)
      WRITE(6,500) ((RR(I),VV(I)),I=1,NPOT)
      READ (5,401) ((ACOEF(J),AEXP(J)),J=1,4)
      WRITE(6,401) ((ACOEF(J),AEXP(J)),J=1,4)
      DO 149 J=1,4
  149 ACOEF(J)= ACOEF(J)*2.*SQRT(AEXP(J))**5/SQRT(3.)
      WRITE (6,507)
      R=RSTART
      V0=(YNTERP(RR,VV,R,NPOT,3)-Z)/R
      READ (5,501) NENG
      DO 941 JJ=1,NENG
      READ (5,502)  EEV
      E = EEV/27.18
      L=0
   18 CONTINUE
C       FINAL WAVEFUNCTION
```

```
      R=RSTART
      LPLUS1=FLOAT(L+1)
      FL=FLOAT(L)
      ALPHA=(Z**2-LPLUS1*(V0+E))/((2.*FL+3.)*LPLUS1)
      BETA=Z*(Z**2-(3.*FL+4.)*(V0+E))/(3.*LPLUS1*(FL+2.)*(2.*FL+3.))
      Y(1)=C*R**LPLUS1*(1.-(Z*R/LPLUS1)+ALPHA*R**2-BETA*R**3)
      Y(2)=C*R**LPLUS1*(-Z/LPLUS1+2.*ALPHA*R-3.*BETA*R**2)
      K=1
      I=1
   20 CALL MODDEQ (DERIV,K,2,R,Y,DY,DR,EPS)
      IF (K .LT.0) GO TO 100
      PHI=Y(1)/R
      XPLT(I)=R
      YPLT(I)=PHI
      I=I+1
      IF (R .LE. RMAX) GO TO 20
      NUM=I-1
      WRITE(6,504) L,NUM
C     INITIAL WAVEFUNCTION
C  SUM OVER BASIS SET, PHINIT(I)=VALUE OF INITIAL WAVEFUNCTION AT R(I)
      IF (JJ.GT.1) GO TO 154
      IF(L.EQ.2) GO TO 154
      TNORM = 0.0
      DO 153 I=1,NUM
      PHINIT(I)=0.0
      DO 151 J=1,4
      S=-AEXP(J)*XPLT(I)
      IF(S.LT.-20.0)  GO TO 151
      PHINIT(I)=PHINIT(I) + XPLT(I)*ACOEF(J)*EXP(S)
  151 CONTINUE
      TNORM=AMAX1(TNORM,PHINIT(I))
  153 CONTINUE
  154 CONTINUE
      SUM=0.0
      IF(L.EQ.0) GO TO 180
      DO 176 I=1,NUM
      TNORM=AMAX1(TNORM,YPLT(I))
      S=YPLT(I)*PHINIT(I)*XPLT(I)**3*DR
      SUM2(I)=S
      SA=ABS(S)
      TES=AMAX1(TES,SA)
      SUM=SUM+S
  176 CONTINUE
      GO TO 39
  180 DO 179 I=1,NUM
      TNORM=AMAX1(TNORM,YPLT(I))
      S=YPLT(I)*PHINIT(I)*XPLT(I)**3*DR
      SUM1(I)=S
      SA=ABS(S)
      TES=AMAX1(TES,SA)
      YPT(I)=YPLT(I)
  179 SUM=SUM+S
      RADINT (1) = SUM
      L=2
      GO TO 18
   39 RADINT (2) = SUM
      WRITE(6,508) EEV,RADINT(1),RADINT(2),TNORM
      WRITE(7,509) EEV, RADINT(1), RADINT(2)
```

```
      DO 177 I=1,NUM
      SUM1(I)=SUM1(I)/TFS
      SUM2(I)=SUM2(I)/TES
      PHINIT(I)=PHINIT(I)/TNORM
      YPLT(I)=YPLT(I)     /TNORM
      YPT(I)=YPT(I)       /TNORM
  177 CONTINUE
      CALL VLABEL(0.,4.,0.,15.,15.,15.,'R (BOHR)',8,0,'(F3.0)',2)
      CALL LABEL(0.,0.,-1.,1.,10.,-1,'C',0,1)
      CALL LABEL(0.,8.5,0.,15.,15.,-15,'PRODUCT',7,0)
      CALL PRTNUM(10.,1.5,0.21,EEV,'(RHENERGY =,F7.3,3H EV)',0.)
      CALL XYPLOT(NUM,XPLT,PHINIT,0.,15.,- 0.8,1.2,DD,0)
      CALL XYPLOT(NUM,XPLT,SUM1,0.,15.,-8.5,1.5,DD,0)
      CALL XYPLOT(NUM,XPLT,SUM2,0.,15.,-8.5,1.5,DD,0)
      CALL XYPLOT(NUM,XPLT,YPT   ,0.,15.,- 0.8,1.2,DD,0)
      CALL XYPLOT(NUM,XPLT,YPLT  ,0.,15.,- 0.8,1.2,DD,1)
  941 CONTINUE
      GO TO 30
  100 CONTINUE
      WRITE (6,530) R,Y(1),DY(1)
      WRITE (6,540) Y(2),DY(2)
      WRITE (6,550)
   30 CONTINUE
      STOP
      END
      SUBROUTINE DERIV (N,R,Y,DY)
      REAL LPLUS1
      INTEGER Z
      COMMON E, LPLUS1, Z, L
      COMMON/VAL/RR,VV,NPOT
      DIMENSION Y(2),DY(2),RR(150),VV(150)
      DY(1)=Y(2)+Y(1)*LPLUS1/R
C
C     INTERPOLATE V FROM TABLE
C
      V=-YNTERP(RR,VV,R,NPOT,3)/R
      DY(2)=2.0*(V-E)*Y(1)-Y(2)*LPLUS1/R
      RETURN
      END
//DATA   DD    *
    8.     OXYGEN
 32       OXYGEN POTENTIAL
0.00031514      7.99604272
0.00066715      7.99160424
0.00124639       7.98426778
0.00263862       7.96648492
0.00318278      7.95948065
0.00408677      7.94778195
0.00524752      7.93265102
0.00673795      7.91305331
0.00865170      7.88763256
0.01340001      7.82348717
0.02075434      7.72185905
0.03214495      7.56143280
0.04677062      7.35465561
0.06805085      7.06054509
0.09301449      6.73382083
0.13533528      6.23175034
```

```
0.18498140      5.71564367
0.25283960      5.10512453
0.34559075      4.41601060
0.47236655      3.71790034
0.60653066      3.16473780
0.82902912      2.45972490
1.13314845      1.80001923
1.54883030      1.26320366
1.75505466      1.08792133
1.86824596      1.01989747
1.98873747      1.0
2.5             1.0
3.0             1.0
4.0             1.0
5.0             1.0
31.10908815     1.0
2P 0.16371         1.15360
2P 0.57600           1.79600
2P  0.33392          3.43790
2P 0.01495         7.90700
  1
  10.0
//
```

Program 2.

```
//RADSULF JOB (98052,WHW,CHE),SHEARD,TIME=(1,50)
/*JOBPARM IOC=15
//       EXEC  FORTG
//SYSPLTDN DD SYSOUT=N
//FORT   DD    *
      REAL LPLUS1
      DIMENSION RADINT(2)
      DIMENSION RR(150),VV(150),Y(2),DY(2)
      DIMENSION DD(3)
      DIMENSION XPLT(800),YPLT(800),PHINIT(800)
      DIMENSION ACOEF(8),AEXP(8)
      DIMENSION YPT(800),SUM1(800),SUM2(800)
      COMMON F,LPLUS1,Z,L
      COMMON/VAL/RR,VV,NPOT
      EXTERNAL DERIV
      DATA DD/0.,0.,0./
  401 FORMAT (2X,2F15.8)
  499 FORMAT(3X,'SULFUR 3P')
  500 FORMAT (2F15.8)
  501 FORMAT (I3)
  502 FORMAT (F7.4)
  503 FORMAT (' ATOMIC NUMBER =', F4.1)
  504 FORMAT (50X,'L =',I3,'     NUM =',I4)
  507 FORMAT (' ENERGY(FV)',11X,'RADINT:  L=0',14X,'L=2')
  508 FORMAT(F15.7,15X,F15.7,2X,E15.7,30X,7HTNORM =,E15.7)
  509 FORMAT (3F15.8)
  530 FORMAT ( 1X,'R=',E18.7,'Y(1)=',E15.7,'DY(1)=',E14.7)
  540 FORMAT ( 21X,'Y(2)=',E15.7,'DY(2)=',E14.7)
  550 FORMAT ( 'ERROR OCCURRED, K=-1, DID NOT CONVERGE')
      N=2
      RSTART=0.003
      C=1.0
      RMAX=15.0
      DR=0.02
      EPS=0.0
      WRITE (6,499)
      WRITE (7,499)
      READ (5,502) Z
      WRITE(6,503)  Z
      READ (5,501) NPOT
      WRITE(6,501) NPOT
      READ (5,500) ((RR(I),VV(I)),I=1,NPOT)
      WRITE(6,500) ((RR(I),VV(I)),I=1,NPOT)
      READ  (5,401) ((ACOEF(J),AEXP(J)),J=1,8)
      WRITE (6,401) ((ACOEF(J),AEXP(J)),J=1,8)
       DO 148 J=1,8
      IF (J.GT.1) GO TO 150
  149 ACOEF(J)= ACOEF(J)*2.*SQRT(AEXP(J))**5/SQRT(3.)
        GO TO 148
  150 ACOEF(J)=ACOEF(J)*0.112687234*SQRT(AEXP(J))**9
  148 CONTINUE
      WRITE (6,507)
      R=RSTART
      V0=(YNTERP(RR,VV,R,NPOT,3)-7)/R
      READ (5,501) NENG
      DO 941 JJ=1,NENG
      READ (5,502)  EEV
      E = EEV/27.18
```

```
      L=0
   18 CONTINUE
C
C       FINAL WAVEFUNCTION
C
      R=RSTART
      LPLUS1=FLOAT(L+1)
      ALPHA=(Z**2-LPLUS1*(V0+E))/((2*L+3)*LPLUS1)
      BETA=Z*(Z**2-(3*L+4)*(V0+E))/(3*LPLUS1*(L+2)*(2*L+3))
      Y(1)=C*R**LPLUS1*(1.-(Z*R/LPLUS1)+ALPHA*R**2-BETA*R**3)
      Y(2)=C*R**LPLUS1*(-Z/LPLUS1+2*ALPHA*R-3*BETA*R**2)
      K=1
      I=1
   20 CALL MODDEQ (DERIV,K,2,R,Y,DY,DR,EPS)
      IF (K .LT.0) GO TO 100
      PHI=Y(1)/R
      XPLT(I)=R
      YPLT(I)=PHI
      I=I+1
      IF (R .LE. RMAX) GO TO 20
      NUM=I-1
      WRITE(6,504) L,NUM
C
C     INITIAL WAVEFUNCTION
C
C  SUM OVER BASIS SET, PHINIT(I)=VALUE OF INITIAL WAVEFUNCTION AT R(I)
C
      IF (JJ.GT.1) GO TO 154
      IF (L.EQ.2) GO TO 154
      TES=0.0
      TNORM = 0.0
      DO 153 I=1,NUM
      PHINIT(I)=0.0
      DO 151 J=1,8
      S=-AEXP(J)*XPLT(I)
      IF(S.LT.-20.0)  GO TO 151
      IF(J.GT.1) GO TO 152
      PHINIT(I)=PHINIT(I)+XPLT(I)*ACOEF(J)*EXP(S)
      GO TO 151
  152 PHINIT(I)=PHINIT(I)+XPLT(I)**3*ACOEF(J)*EXP(S)
  151 CONTINUE
      TNORM=AMAX1(TNORM,PHINIT(I))
  153 CONTINUE
  154 CONTINUE
      SUM=0.0
      IF(L.EQ.0) GO TO 175
      DO 176 I=1,NUM
      TNORM=AMAX1(TNORM,YPLT(I))
      S=YPLT(I)*PHINIT(I)*XPLT(I)**3*DR
      SUM2(I)=S
      SA=ABS(S)
      TES=AMAX1(TES,SA)
      SUM=SUM+S
  176 CONTINUE
      GO TO 39
  175 DO 178 I=1,NUM
      TNORM=AMAX1(TNORM,YPLT(I))
      S=YPLT(I)*PHINIT(I)*XPLT(I)**3*DR
```

```
      SUM1(I)=S
      SA=ABS(S)
      TES=AMAX1(TES,SA)
      SUM=SUM+S
      YPT(I)=YPLT(I)
  178 CONTINUE
      RADINT (1) = SUM
      L=2
      GO TO 18
   39 RADINT (2) = SUM
      WRITE(6,508) EEV,RADINT(1),RADINT(2),TNORM
      WRITE(7,509) EEV, RADINT(1), RADINT(2)
      DO 177 I=1,NUM
      SUM1(I)=SUM1(I)/TES
      SUM2(I)=SUM2(I)/TES
      PHINIT(I)=PHINIT(I)/TNORM
      YPLT(I)=YPLT(I)     /TNORM
      YPT(I)=YPT(I)       /TNORM
  177 CONTINUE
      CALL VLABEL(0.,4.,0.,15.,15.,15,'R (BOHR)',8,0,'(F3.0)',2)
      CALL LABEL(0.,8.5,0.,15.,15.,-15,'PRODUCT',7,0)
      CALL LABEL(0.,0.,-1.,1.,10.,-1,'C',0,1)
      CALL PRTNUM(10.,1.5,0.21,EEV,'(8HENERGY =,F7.3,3H EV)',0.)
      CALL XYPLOT(NUM,XPLT,PHINIT,0.,15.,-0.8,1.2,DD,0)
      CALL XYPLOT(NUM,XPLT,SUM1,0.,15.,-8.5,1.5,DD,0)
      CALL XYPLOT(NUM,XPLT,YPT   ,0.,15.,-0.8,1.2,DD,0)
      CALL XYPLOT(NUM,XPLT,SUM2,0.,15.,-8.5,1.5,DD,0)
      CALL XYPLOT(NUM,XPLT,YPLT  ,0.,15.,-0.8,1.2,DD,1)
  941 CONTINUE
      GO TO 30
  100 CONTINUE
      WRITE (6,530) R,Y(1),DY(1)
      WRITE (6,540) Y(2),DY(2)
      WRITE (6,550)
   30 CONTINUE
      STOP
      END
      SUBROUTINE DERIV (N,R,Y,DY)
      REAL LPLUS1
      COMMON E,LPLUS1,Z,L
      COMMON/VAL/RR,VV,NPOT
      DIMENSION Y(2),DY(2),RR(150),VV(150)
      DY(1)=Y(2)+Y(1)*LPLUS1/R
C
C     INTERPOLATE V FROM TABLE
C
      V=-YNTERP(RR,VV,R,NPOT,3)/R
      DY(2)=2.0*(V-E)*Y(1)-Y(2)*LPLUS1/R
      RETURN
      END
//DATA   DD    *
   16.     SULFUR
 42       SULFUR POTENTIAL
0.00031514      15.98761569
0.00066715      15.97368449
0.00124639      15.95061087
0.00263862      15.89453639
0.00318278      15.87241337
```

```
0.00408677      15.83543696
0.00524752      15.78759037
0.00673795      15.72563318
0.00865170      15.64537966
0.01340001      15.44403079
 0.02075434     15.13026175
0.03214495      14.65118778
0.04677062      14.06279503
0.06805085      13.27077097
0.09301449      12.43093849
0.13533528      11.19515295
0.18498140      10.01485846
0.20961139      9.51604911
 0.25283960     8.74027206
0.30498277      7.93620896
0.34559075      7.39296651
0.39160563      6.85242783
0.47236655      6.05961474
0.53526143      5.54651371
0.60653066      5.04499272
0.68728928      4.55597903
 0.82902912      3.86922589
1.00000000      3.28670529
1.13314845      2.94989331
1.54883030      2.17381205
1.75505466      1.88692895
1.86824596      1.75148796
1.98873747      1.62224996
 2.11700002     1.49960568
2.25353479      1.38373585
2.39887529      1.27466702
2.55358946      1.17232375
2.71828183      1.07660582
2.89359594      1.01137375
3.08021685      1.0
9.00            1.0
31.0            1.0
2P  -0.15546        8.0000                      S
4P  -0.00995       14.12590                     S
4P   0.01287       11.57180
4P  -0.09992        7.91710              S
4P   0.05174        5.60390              S
4P   0.55282        2.89060              S
4P   0.50896        1.62750              S
4P   0.02556        0.86650              S
  1
  10.0
//
```

Program 3.

```
//ANGSUL JOB (98052,WHW,CHE),'S. SHEARD',TIME=(1,59)
/*JOBPARM IOC=40,LINES=4,PLT=480
//       EXEC  FORTG
//SYSPLTDN DD SYSOUT=N
//FORT   DD    *
C       INPUT CARDS
C       1.  COEFFICIENTS OF INITIAL STATE P FUNCTIONS Y(1,-1), Y(1,0), AND
C       Y(1,+1) IN COMPLEX FORM.  (YINM(3), FORMAT 6F10.3).
C
C       2.  NUMBER OF RADIAL INTEGRALS SUPPLIED FROM RADIAL PROGRAMS.
C       (NRAD, FORMAT I3)
C       3.  ENERGIES AND RADIAL INTEGRALS (ENERGY(I), SDUM(I), AND KDUM(I),
C       FORMAT 3E15.8)
C       THERE MUST BE EXACTLY NRAD OF THESE CARDS.
C       4.  PLOTTING INFORMATION:  1 CARD FOR NUMBER OF PLOTS PER ENERGY
C       AND POLARIZATION, UP TO 10.  (NPLOT, FORMAT I3)
C       5.  FOR EACH PLOT:  WHICH PLOT (LPLOT, AS DESCRIBED BELOW), STEP
C       SIZE OF VARYING ANGLE (ANSTEP),VALUE FOR FIXED ANGLE (ANGFIX),
C       AND IF LPLOT4 OR 8, MINIMUM AND MAXIMUM OF VARYING ANGLE (ANGMIN
C       AND ANGMAX).  (FORMAT I3,4F10.7)
C      LPLOT=1, THETA = 0 TO 90              LPLOT=5, PHI = 0 TO 90
C      LPLOT=2, THETA = 0 TO 180             LPLOT=6, PHI = 0 TO 180
C      LPLOT=3, THETA = 0 TO 360             LPLOT=7, PHI = 0 TO 360
C      LPLOT=4, THETA = OTHER RANGE          LPLOT=8, PHI = OTHER RANGE
C       6.  NUMBER OF ENERGIES AT WHICH THE DISTRIBUTIONS WILL BE CALCULATED
C       (NENG, FORMAT I3)
C       7.  FINAL STATE ELECTRON KINETIC ENERGIES, IN ELECTRON VOLTS.  (EEV,
C       FORMAT F10.3)
C       THERE MUST BE AT LEAST NENG OF THESE CARDS.  ONLY THE FIRST NENG OF
C       THEM WILL BE READ
C
      DIMENSION ENG(11,2),DETR(11,15,2)
      DIMENSION A(3),RADINT(2)
      DIMENSION CUR(80),PANGLE(80),AANGLE(80)
      DIMENSION X(80),Y(80)
      DIMENSION XA(80,2,5),P(80,5),Q(80,5)
      DIMENSION NP(5)
      DIMENSION DPLT(11),EPLT(11)
      DIMENSION DD(3)
      DIMENSION LPLOT(5),ANSTEP( 5),ANGFIX(5),ANGMAX(5),ANGMIN(5)
      DIMENSION ENERGY(30),SDUM(30)
      REAL KDUM(30)
      COMPLEX YINM(3),CYLM(6),ANGINT(3,3,5),CI,PSIF,YLM(6)
      COMMON /RADI/ENERGY,SDUM,KDUM
      DATA DD/0.,0.,0./
  102 FORMAT(6F10.3)
  103 FORMAT(3X,'UNPOLARIZED LIGHT TRAVELING IN Z DIRECTION')
  104 FORMAT (I3,4F10.7)
  105 FORMAT (I3)
  106 FORMAT ( ' PLOT#  LPLOT    ANGFIX     ANGMIN     ANGMAX     ANSTEP  ')
  107 FORMAT (I4,I7,4F10.3)
  108 FORMAT(3E15.8)
  109 FORMAT(3X,'ENERGY =',F8.3,' EV')
  110 FORMAT(3X,'X POLARIZATION')
  111 FORMAT(3X,'Z POLARIZATION')
  113 FORMAT(3X,3E15.8)
  508 FORMAT (22X,'POLAR ANGLE',17X,'AZIMUTHAL ANGLE',14X,
     &'DETECTOR INTENSITY')
```

```
  509 FORMAT (25X,'THETA',26X,'PHI',23X,'I(THETA,PHI)'/)
  510 FORMAT (15X,F15.1,15X,F15.1,18X,E15.7)
      PI=3.141593
      Y1=SQRT(1.0/(4.0*PI))
      Y2=SQRT(45./(96.*PI))
      Y3=SQRT(45./(24.*PI))
      Y4=SQRT(5.0/(4.0*PI))
      RAD=PI/180.0
      CT=(0.0,1.0)
C
C
C  GENERATE ANGINT TENSOR
C     ANGULAR INTEGRALS FROM CLEBSCH-GORDAN COEFFICIENTS
C
       ANGINT(1,1,1)=(  -0.4082482,   0.0       )
       ANGINT(2,1,1)=(   0.0       ,   0.4082482)
       ANGINT(3,1,1)=(   0.0       ,   0.0       )
       ANGINT(1,2,1)=(   0.0       ,   0.0       )
       ANGINT(2,2,1)=(   0.0       ,   0.0       )
       ANGINT(3,2,1)=(   0.5773503,   0.0       )
       ANGINT(1,3,1)=(   0.4082482,   0.0       )
       ANGINT(2,3,1)=(   0.0       ,   0.4082482)
       ANGINT(3,3,1)=(   0.0       ,   0.0       )
       ANGINT(1,1,2)=(  -0.4472136,   0.0       )
       ANGINT(2,1,2)=(   0.0       ,  -0.4472136)
       ANGINT(3,1,2)=(   0.0       ,   0.0       )
       ANGINT(1,2,2)=(   0.0       ,   0.0       )
       ANGINT(2,2,2)=(   0.0       ,   0.0       )
       ANGINT(3,2,2)=(   0.0       ,   0.0       )
       ANGINT(1,3,2)=(   0.0       ,   0.0       )
       ANGINT(2,3,2)=(   0.0       ,   0.0       )
       ANGINT(3,3,2)=(   0.0       ,   0.0       )
       ANGINT(1,1,3)=(   0.0       ,   0.0       )
       ANGINT(2,1,3)=(   0.0       ,   0.0       )
       ANGINT(3,1,3)=(   0.4472136,   0.0       )
       ANGINT(1,2,3)=(  -0.3162278,   0.0       )
       ANGINT(2,2,3)=(   0.0       ,  -0.3162278)
       ANGINT(3,2,3)=(   0.0       ,   0.0       )
       ANGINT(1,3,3)=(   0.0       ,   0.0       )
       ANGINT(2,3,3)=(   0.0       ,   0.0       )
       ANGINT(3,3,3)=(   0.0       ,   0.0       )
       ANGINT(1,1,4)=(   0.1825742,   0.0       )
       ANGINT(2,1,4)=(   0.0       ,  -0.1825742)
       ANGINT(3,1,4)=(   0.0       ,   0.0       )
       ANGINT(1,2,4)=(   0.0       ,   0.0       )
       ANGINT(2,2,4)=(   0.0       ,   0.0       )
       ANGINT(3,2,4)=(   0.5163978,   0.0       )
       ANGINT(1,3,4)=(  -0.1825742,   0.0       )
       ANGINT(2,3,4)=(   0.0       ,  -0.1825742)
       ANGINT(3,3,4)=(   0.0       ,   0.0       )
       ANGINT(1,1,5)=(   0.0       ,   0.0       )
       ANGINT(2,1,5)=(   0.0       ,   0.0       )
       ANGINT(3,1,5)=(   0.0       ,   0.0       )
       ANGINT(1,2,5)=(   0.3162278,   0.0       )
       ANGINT(2,2,5)=(   0.0       ,  -0.3162278)
       ANGINT(3,2,5)=(   0.0       ,   0.0       )
       ANGINT(1,3,5)=(   0.0       ,   0.0       )
       ANGINT(2,3,5)=(   0.0       ,   0.0       )
```

```
      ANGINT(3,3,5)=(   0.4472136,   0.0       )
      ANGINT(1,1,6)=(   0.0       ,   0.0       )
      ANGINT(2,1,6)=(   0.0       ,   0.0       )
      ANGINT(3,1,6)=(   0.0       ,   0.0       )
      ANGINT(1,2,6)=(   0.0       ,   0.0       )
      ANGINT(2,2,6)=(   0.0       ,   0.0       )
      ANGINT(3,2,6)=(   0.0       ,   0.0       )
      ANGINT(1,3,6)=(   0.4472136,   0.0       )
      ANGINT(2,3,6)=(   0.0       ,  -0.4472136)
      ANGINT(3,3,6)=(   0.0       ,   0.0       )
C
C
      READ(5,102) YINM
      READ (5,105) NPLOT
      DO 19 IJ=1,NPLOT
      READ(5,104) LPLOT(IJ),ANSTEP(IJ),ANGFIX(IJ),ANGMIN(IJ),ANGMAX(IJ)
   19 CONTINUE
C
C    ENERGY LOOP
C
      READ(5,105) NENG
      DO 771 IENG=1,NENG
      READ (5,108) EEV,RADINT(1),RADINT(2)
      WRITE(6,113) EEV,RADINT(1),RADINT(2)
C
C     POLARIZATION LOOP
C     FOR UNPOLARIZED LIGHT
C
      A(2)=(0.,0.)
      DO  772 IPOL=1,3
      GO TO (690,691,693),IPOL
  690 A(1)=(1.,0.)
      A(3)=(0.,0.)
      WRITE(6,110)
      GO TO 692
  691 A(1)=(0.0,0.0)
      A(3)=(1.,0.)
      WRITE(6,111)
  692 CONTINUE
C  CALCULATE THE SUM OVER INITIAL STATES OF THE ANGULAR INTEGRAL
C
      DO 20 J=1,6
      CYLM(J)=(0.0,0.0)
      DO 15 IX=1,3
      DO 15 IB=1,3
   15 CYLM(J)=CYLM(J)+A(IX)*ANGINT(IX,IB,J)*YINM(IB)
C
C  MULTIPLY BY RADINT.  TOTAL DETECTOR INTENSITY IS PROPORTIONAL TO
C     THIS RESULT TIMES THE SPHERICAL HARMONICS Y (L,M)
C      EVALUATED AT THETA AND PHI.
C
      CYLM(J)=RADINT(2)*CYLM(J)
      IF (J.EQ.1) CYLM(J)=RADINT(1)*CYLM(J)/RADINT(2)
   20 CONTINUE
C
C       EVALUATE Y(L,M) AT ANGLES FOR PLOT
C
  693 CONTINUE
```

```
      DO 55 IJ=1,NPLOT
      LPT=LPLOT(IJ)
      GO TO (122,122,125),IPOL
  122 CONTINUE
      GO TO (21,22,23,24,21,22,23,24),LPT
   21 ANGMIN(IJ)=0.0
      ANGMAX(IJ)=90.0
      GO TO 24
   22 ANGMIN(IJ)=0.0
      ANGMAX(IJ)=180.
      GO TO 24
   23 ANGMIN(IJ)=0.
      ANGMAX(IJ)=360.
   24 CONTINUE
      WRITE (6,106)
      WRITE(6,107) IJ,LPLOT(IJ),ANGFIX(IJ),ANGMIN(IJ),
     & ANGMAX(IJ),ANSTEP(IJ)
      WRITE(6,508)
      WRITE(6,509)
      GO TO (25,25,25,25,26,26,26,26),LPT
   25 CONTINUE
C
C  SWEEP THETA WHILE HOLDING PHI FIXED
C
C  ZERO ANGLES
C
      PO=ANGMIN(IJ)-ANSTEP(IJ)
      AZ=ANGFIX(IJ)
      I=0
   37 CONTINUE
C
C  LOOP OVER THETA
C
      PO=PO+ANSTEP(IJ)
      I=I+1
      ANGVAR=PO
      GO TO 39
   26 CONTINUE
C
C  SWEEP PHI WHILE HOLDING THETA FIXED
C
C  ZERO ANGLES
C
      PO=ANGFIX(IJ)
      AZ=ANGMIN(IJ)-ANSTEP(IJ)
      I=0
   38 CONTINUE
C
C  LOOP OVER PHI
C
      AZ=AZ+ANSTEP(IJ)
      I=I+1
      ANGVAR=AZ
   39 CONTINUE
      PSIF=(0.0,0.0)
C
C  CALCULATE VALUES OF THE SPHERICAL HARMONICS AT THETA AND PHI
C     J=1:  L,M=0;   J=2 TO 6:  L=2, M=-2 TO 2
```

```
C
      CPO=COS(PO*RAD)
      SPO=SIN(PO*RAD)
      CAZ=COS(AZ*RAD)
      SAZ=SIN(AZ*RAD)
      C2AZ=COS(2.*AZ*RAD)
      S2AZ=SIN(2.*AZ*RAD)
      YLM(1)=Y1
      YLM(2)=Y2*SPO**2*(C2AZ-CI*S2AZ)
      YLM(3)=Y3*SPO*CPO*(CAZ-CI*SAZ)
      YLM(4)=Y4*(1.5*CPO**2-0.5)
      YLM(5)=-Y3*SPO*CPO*(CAZ+CI*SAZ)
      YLM(6)=Y2*SPO**2*(C2AZ+CI*S2AZ)
      DO 48 J=1,6
      PSIF=PSIF+CYLM(J)*YLM(J)
C     WRITE (6,201) YLM,PSIF,J,CYLM(J)
C 201 FORMAT (' YLM=' ,2F12.5,'    PSIF=',2F12.5,'    CYLM(',
C    &I1,')=',2F12.5)
   48 CONTINUE
C
C  DETECTOR INTENSITY = 'CUR'
C
      CUR(I)=REAL(PSIF*CONJG(PSIF))
      XA(I,IPOL,IJ)=CUR(I)
   50 CONTINUE
      PANGLE(I)=PO
      AANGLE(I)=AZ
      P(I,IJ)=PANGLE(I)
      Q(I,IJ)=AANGLE(I)
      WRITE (6,510) PANGLE(I),AANGLE(I),CUR(I)
      IF (ANGVAR.GE.ANGMAX(IJ)) GO TO 53
C
C  RETURN FOR NEXT ANGLE
C
      GO TO (37,37,37,37,38,38,38,38),LPT
   53 CONTINUE
      NPOIN=I
      NP(IJ)=NPOIN
C
C  FIND MAXIMUM DETECTOR CURRENT
C
      TEST=CUR(1)
      DO 60 K=2,NPOIN
      XA(K,IPOL,IJ)=CUR(K)
      IF(CUR(K)-TEST) 60,60,58
   58 TEST=CUR(K)
   60 CONTINUE
      GO TO 120
C       FOR UNPOLARIZED LIGHT
  125 CONTINUE
      NPOIN=NP(IJ)
  121 TEST=0.0
      WRITE(6,103)
      WRITE(6,106)
      WRITE(6,107) IJ,LPLOT(IJ),ANGFIX(IJ),ANGMIN(IJ),ANGMAX(IJ),
     & ANSTEP(IJ)
      WRITE(6,508)
      WRITE(6,509)
```

```
      DO 123 K=1,NPOIN
      XA(K,1,IJ)=XA(K,1,IJ)+XA(K,2,IJ)
      PANGLE(K)=P(K,IJ)
      AANGLE(K)=Q(K,IJ)
      CUR(K)=XA(K,1,IJ)
      WRITE(6,510) PANGLE(K),AANGLE(K),XA(K,1,IJ)
      IF(XA(K,1,IJ)-TEST)123,123,124
  124 TEST=XA(K,1,IJ)
  123 CONTINUE
  120 CONTINUE
C
C  NORMALIZE CURRENT
C
      DO 62 K=1,NPOIN
   62 CUR(K)=CUR(K)/TEST
C
C        PLOT
C
      CALL PRTNUM (10.,2.,0.21,EEV,'(8HENERGY =,F7.3,3H EV)',0.)
      IF(IPOL-2) 10,11,12
   10 CALL SYSSYM(10.,1.5,0.21,'X POLARIZATION',14,0.)
      GO TO 13
   11 CALL SYSSYM(10.,1.5,0.21,'Z POLARIZATION',14,0.)
      GO TO 13
   12 CALL SYSSYM(10.,1.5,0.21,'UNPOLARIZED LIGHT',17,0.)
   13 CONTINUE
      GO TO (63,64,65,65,66,67,68,68),LPT
C
C   LPLOT = 1
C
   63 CONTINUE
      DO 81 K=1,NPOIN
      X(K)=CUR(K)*SIN(PANGLE(K)*RAD)
      Y(K)=CUR(K)*COS(PANGLE(K)*RAD)
   81 CONTINUE
      CALL VLABEL(3.,3.,0.,1.,5.,1,'CURRENT',7,0,'(F2.0)',1)
      CALL VLABEL(3.,3.,0.,1.,5.,1,'CURRENT',7,1,'(F2.0)',1)
      CALL PRTNUM(10.0,8.0,0.21,AANGLE,'(5HPHI =,F5.1,8H DEGREES)',0.)
      CALL SYSSYM(10.,8.5,0.21,'THETA = 0 TO 90 DEGREES',23,0.)
      CALL XYPLOT(NPOIN,X,Y,-0.6,2.4,-0.6,1.4,DD,1)
      GO TO 54
C
C   LPLOT = 2
C
   64 CONTINUE
      DO 82 K=1,NPOIN
      X(K)=CUR(K)*SIN(PANGLE(K)*RAD)
      Y(K)=CUR(K)*COS(RANGLE(K)*RAD)
   82 CONTINUE
      CALL VLABEL(2.,8.,0.,1.,2.,1,'CURRENT',7,0,'(F2.0)',1)
      CALL LABEL(2.,6.,-1.,1., 4.,-2,'CURRENT',0,1)
      CALL PRTNUM(10.0,8.0,0.21,AANGLE,'(5HPHI =,F5.1,8H DEGREES)',0.)
      CALL SYSSYM(10.,8.5,0.21,'THETA = 0 TO 180 DEGREES',24,0.)
      CALL XYPLOT (NPOIN,X,Y,-1.,6.5,-4.,1.,DD,0)
      GO TO 54
```

```
C
C   LPLOT = 3 OR 4

      DO 83 K=1,NPOIN
      X(K)=CUR(K)*SIN(PANGLE(K)*RAD)
      Y(K)=CUR(K)*COS(PANGLE(K)*RAD)
   83 CONTINUE
      CALL LABFL(1.,5.,-1.,1.,10.,-2,'CURRENT',0,0)
      CALL LABEL(6.,0.,-1.,1.,10.,-2,'CURRENT',0,1)
      CALL PRTNUM(10.0,8.0,0.21,AANGLE,'(5HPHI =,F5.1,8H DEGREES)',0.)
      IF (LPLOT(IJ).EQ.4) GO TO 51
      CALL SYSSYM(10.,8.5,0.21,'THETA = 0 TO 360 DEGREES',24,0.)
   51 CONTINUE
      CALL XYPLOT (NPOIN,X,Y,-1.2,1.8,-1.0,1.0,DD,1)
      GO TO 54
C
C   LPLOT = 5
C
   66 CONTINUE
      DO 84 K=1,NPOIN
      Y(K)=CUR(K)*SIN(AANGLE(K)*RAD)
      X(K)=CUR(K)*COS(AANGLE(K)*RAD)
   84 CONTINUE
      CALL VLABEL(3.,3.,0.,1.,5.,1,'CURRENT',7,0,'(F2.0)',1)
      CALL VLABEL(3.,3.,0.,1.,5.,1,'CURRENT',7,1,'(F2.0)',1)
      CALL PRTNUM(10.,8.00,0.21,PANGLE,'(7HTHETA =,F5.1,8H DEGREES)',0.)
      CALL SYSSYM(10.0,8.5,0.21,'PHI = 0 TO 90 DEGREES',21,0.)
      CALL XYPLOT (NPOIN,X,Y,-.6,2.4,-.6,1.4,DD,1)
      GO TO 54
C
C   LPLOT = 6
C
   67 CONTINUE
      DO 85 K=1,NPOIN
      Y(K)=CUR(K)*SIN(AANGLE(K)*RAD)
      X(K)=CUR(K)*COS(AANGLE(K)*RAD)
   85 CONTINUE
      CALL LABEL(6.,3.,0.,1.,5.,-1,'CURRENT',0,1)
      CALL PRTNUM(10.,8.00,0.21,PANGLE,'(7HTHETA =,F5.1,8H DEGREES)',0.)
      CALL SYSSYM(10.0,8.5,0.21,'PHI = 0 TO 180 DEGREES',22,0.)
      CALL XYPLOT(NPOIN,X,Y,-1.2,1.8,-.6,1.4,DD,1)
      GO TO 54
C
C   LPLOT = 7 OR 8
C
   68 CONTINUE
      DO 86 K=1,NPOIN
      Y(K)=CUR(K)*SIN(AANGLE(K)*RAD)
      X(K)=CUR(K)*COS(AANGLE(K)*RAD)
   86 CONTINUE
      CALL LABEL(0.,3.,-1.,1., 4.,-2,'CURRENT',0,0)
      CALL LABFL(2.,1.,-1.,1., 4.,-2,'CURRENT',0,1)
      CALL PRTNUM(10.,3.50,0.21,PANGLE,'(7HTHETA =,F5.1,8H DEGREES)',0.)
      IF (LPLOT(IJ).EQ.8) GO TO 52
      CALL SYSSYM(10.0,4.0,0.21,'PHI = 0 TO 360 DEGREES',22,0.)
   52 CONTINUE
      CALL XYPLOT (NPOIN,X,Y,-1.0,6.5,-1.5,3.5,DD,1)
```

```
   54 CONTINUE
   55 CONTINUE
  772 CONTINUE
  771 CONTINUE
  200 CONTINUE
  100 STOP
      END
      SUBROUTINE RADIAL(E,FS,FK,NRAD)
      DIMENSION ENERGY(30),SDUM(30)
      REAL KDUM(30)
      COMMON /RADI/ ENERGY,SDUM,KDUM
      FS=YNTERP(ENERGY,SDUM,E,NRAD,3)
      FK=YNTERP(ENERGY,KDUM,E,NRAD,3)
      RETURN
      END
//DATA   DD    *
                          1.0
  2   SULFUR
  2  5.0       0.0
  7  5.0      10.0
  5
 0.10000000E 01-0.22142375E 00 0.11007625E 00
 0.10000000E 02-0.10206109E 00 0.14456525E-01
 0.25000000E 02-0.42851407E-01-0.29119879E-02
 0.50000000E 02-0.18469468E-01-0.29701153E-02
 0.10000000E 03-0.67723021E-02-0.12967903E-02
//
```

Program 4.

```
//RADTABLE JOB (9R05?,WHW,CHE),SHEARD,TIME=(1,40)
/*JOBPARM IOC=15
//       EXEC  FORTG
//SYSPLTON DD SYSOUT=N
//FORT   DD    *
C
C       THIS PROGRAM LISTS AND PLOTS RADIAL INTEGRALS VS. ENERGY
C       FOR UP TO 8 ATOMS,UP TO 50 ENERGIES PER ATOM.
C
C       THERE ARE 4 ATOMS TO A GRAPH SHEET, WITH THE TOP GRAPH BEING
C       RADINT(1), THE MIDDLE BEING RADINT(2), AND THE BOTTOM BEING
C       RADINT(2)/RADINT(1), MAKING A TOTAL OF 12 GRAPHS PER SHEET.
C
C       NATM IS THE NUMBER OF ATOMS, I INDEXES THEM, AND IATM
C       INDEXES THE ATOMS ON ANY ONE GRAPH SHEET.
C
C       NENG (= NE(I)) IS THE NUMBER OF ENERGIES FOR WHICH THERE ARE
C       RADIAL INTEGRALS FOR ATOM I
C
C       INPUT NATM, THEN NENG FOR EACH ATOM (FORMAT(I3),ONE CARD EACH),
C       THEN INPUT ENERGIES AND RADIAL INTEGRALS FROM RADINTS PROGRAM
C       (PUNCHED CARDS). FORMAT (3E15.8)
C
C       THE ENERGIES ARE ASSUMED TO COVER 0 TO 100 EV
C
C       EPLT IS THE X-AXIS MATRIX AND DPLT IS THE Y-AXIS MATRIX
C
      DIMENSION ENERGY (8,50),RAD1(8,50),RAD2(8,50),RAD3(8,50)
      DIMENSION NE(8)
      DIMENSION YMP(3),YPP(3)
      DIMENSION X(4),Y(3),DPLT(50),EPLT(50)
      DIMENSION XMINP(4),XMAXP(4),YMINP(3),YMAXP(3)
      DIMENSION DD (3)
       INTEGER TEST
      DATA X/2.,5.,8.,11./
      DATA Y/7.,4.,1./
      DATA XMINP/-100.,-250.,-400.,-550./
      DATA XMAXP/650.,500.,350.,200./
      DATA YMINP/-0.35,-0.20,-0.5/
      DATA YMAXP/0.15,0.30,4.5/
      DATA YPP/0.10,0.1,1.0/
      DATA YMP/0.0,0.0,0.0/
      DATA DD /0.0,0.0,0.0/
C
C       X(I) AND Y(J) ARE THE AXIS STARTING POINTS FOR THE GRAPH IN THE ITH
C       COLUMN AND THE JTH ROW
C
C       XMINP(I) AND YMINP(I) ARE THE VALUES OF THE LEFT AND RIGHT HAND
C       EDGES OF THE PLOTTING AREAS FOR THE ITH COLUMN OF GRAPHS ON THE PAGE
C
C       YMINP(I) AND YMAXP(I) ARE THE VALUES OF THE TOP AND BOTTOM OF THE PAGE
C       FOR THE ITH ROW OF GRAPHS.  THESE MUST BE ADJUSTED EACH TIME YOU
C       CHANGE VERTICAL SCALES ON THE GRAPH AXES.
C
C       YMP(I) AND YPP(I) ARE THE UPPER AND LOWER VALUES OF THE AXES FOR THE
C       ITH ROW OF GRAPHS.  CHANGING THESE CHANGES THE ORIGIN AND THE VERTICAL
C       SCALE.  THEY AFFECT ONLY THE AXIS PLOTTING, NOT THE LINE PLOTTING.
C
```

```
201 FORMAT (3F15.8)
202 FORMAT(I3)
203  FORMAT ('  NATM =',I3)
204 FORMAT(21X,'ATOM NO.',I2,59X,'ATOM NO.',I2)
205 FORMAT (6X,'ENG',8X,'RAD1',8X,'RAD2',8X,'RAD3',29X,'ENG',8X,
   &  'RAD1',8X,'RAD2',8X,'RAD3')
206 FORMAT (F12.6,3E12.5,20X,F12.6,3E12.5)
207 FORMAT(21X,'ATOM NO.',I2)
208 FORMAT(6X,'ENG',8X,'RAD1',8X,'RAD2',8X,'RAD3')
209 FORMAT(F12.6,3E12.5)
210 FORMAT('  NENG =',I3)
    READ (5,202) NATM
    WRITE   (6,203) NATM
    TEST=0.0
    DO 161 I=1,NATM
    READ(5,202) NENG
    WRITE(6,210) NENG
     NE(I)=NENG
    TEST=MAX0(TEST,NENG)
161 CONTINUE
    DO 160 I=1,NATM
    NENG=NE(I)
    DO 130 J=1,NENG
    READ(5,201) ENERGY(I,J),RAD1(I,J),RAD2(I,J)


    RAD3(I,J)=RAD2(I,J)/RAD1(I,J)
130 CONTINUE
    K=NENG+1
    IF (NENG.EQ.TEST) GO TO 160
    DO 140 J=K,TEST
    ENERGY(I,J)=0.0
    RAD1(I,J)=1.
    RAD2(I,J)=1.
    RAD3(I,J)=1.
140 CONTINUE
160 CONTINUE
    DO 190 JJ=1,20
    IE=(NATM+1)/2
    IF(JJ.GT.IE) GO TO 190
    ID=NATM/2
    IF(JJ.GT.ID) GO TO 180
    JK=JJ*2
    JI=JK-1
    WRITE(6,204) JI,JK
    WRITE(6,205)
    DO 150 J=1,TEST
    WRITE (6,206) ENERGY(JI,J),RAD1(JI,J),RAD2(JI,J),RAD3(JI,J),
   & ENERGY(JK,J),RAD1(JK,J),RAD2(JK,J),RAD3(JK,J)
150 CONTINUE
    GO TO 190
180 CONTINUE
    JI=JJ*2-1
    WRITE(6,207) JI
    WRITE(6,208)
    DO 155 J=1,TEST
    WRITE(6,209) ENERGY(JI,J),RAD1(JI,J),RAD2(JI,J),RAD3(JI,J)
155 CONTINUE
```

```
  190 CONTINUE
      DO 301 I=1,NATM
      LABL=0
      IATM=I
      IF (I.GT.3) IATM=I-3
      IF(IATM.GT.1) GO TO 311
      CALL SYSSYM(0.25,9.39,0.21,'ATOM',4,0.)
      CALL SYSSYM(0.25,8.1,0.21,'L=0',3,0.)

      CALL SYSSYM(0.25,5.1,0.21,'L=2',3,0.)

      CALL SYSSYM(0.25,2.1,0.21,'RATIO',5,0.)

      CALL SYSSYM(2.9, 9.39,0.21,'ST',2,0.)
  311 CONTINUE

C
C       FOR EACH ATOM:
C
      STARTX=(FLOAT(IATM)*3.)-0.05
      STARTX=X(IATM)
      NENG=NE(I)
      DO 304  KC=1,NENG
      EPLT(KC)=ENERGY(I,KC)
  304 CONTINUE
      XM=XMINP(IATM)
      XX=XMAXP(IATM)
C
C       FOR EACH GRAPH RELATED TO THAT ATOM:
C
      DO 302 IPLT=1,3
      GO TO (305,306,307),IPLT
  305 DO 303 KC=1,NENG
  303 DPLT(KC)=RAD1(I,KC)
      GO TO 308
  306 DO 309 KC=1,NENG
  309 DPLT(KC)=RAD2(I,KC)
      GO TO 308
  307 DO 310  KC=1,NENG
  310 DPLT(KC)=RAD3(I,KC)
      IF(IATM.EQ.3) LABL=-1
C
C       THIS MEANS THE LAST GRAPH ON THE SHEET
C
  308 CONTINUE
      STARTY=Y(IPLT)
      YM=YMINP(IPLT)
      YX=YMAXP(IPLT)
      YMN=YMP(IPLT)
      YMX=YPP(IPLT)
      STRTY=Y(IPLT)
C
      CALL VLABEL(STARTX,STARTY,0.,100.,2.,2,'ENERGY (EV)',11,0,
     & '(FS.0)',4)
      CALL VLABEL(STARTX,STARTY,YMN,YMX,2.,2,'C',0,1,'(F6.3)',6)
      CALL XYPLOT(NENG,EPLT,DPLT,XM,XX,YM,YX,DD,LABL)
  302 CONTINUE
  301 CONTINUE
      STOP
      END
//DATA   DD     *
```

APPENDIX 2

Laser-Induced Chemisorption Studies

This work occupied much of the actual time of my master's work. The project consisted mainly of constructing the vacuum system used. However, since no experiments have been completed as of this time, this work is included only as an appendix. The work will be completed by others in the future.

Surface studies attempt to understand the nature of bonding between solids and the species adsorbed on them. An important area of investigation is the characteristics of the activation energy barrier to adsorption of saturated hydrocarbons on transition metals. This research has important implications in the field of industrial catalysis. One would like to know what type of energy is needed when a molecule sticks to a surface and dissociates: is it translational, rotational, or vibrational energy of the gas molecule or vibrational energy of the surface?

The answers to these questions are well developed for the specific system of methane on rhodium. In a novel series of careful experiments, Charles Stewart and Gert Ehrlich[1] used a heated molecular beam of methane directed at a rhodium field emission tip to measure adsorption rates for three isotopes of methane, CH_4, CH_2D_2, and CD_4. Analysis of the isotope data ruled out translational energy, surface residence lifetime, electronic or rotational energies as determining adsorption probabilities. Two methods of vibrational analysis were then applied to the data to determine which of the vibrational modes was most likely to be responsible. Of these methods, the better accepted RRKM activated complex theory made predictions that were in poor agreement with the results, although rates calculated for the ν_3 asymmetric stretch (see Fig. 1) agreed least poorly. Slater's dynamical model of unimolecular reactions, which uses bond extension due to a random superposition of normal vibrational modes as the critical factor for dissociation, appeared to agree much more closely with the results. From this analysis, Stewart and Ehrlich concluded that the active vibrational mode is ν_4, an asymmetric bend in which the mean square

displacement of the hydrogen-hydrogen distances is a maximum. Such a mode would show appreciable isotope effects since the heavier deuterium atoms would not vibrate so far.

Our experiment was designed to test whether the ν_3 or ν_4 vibrationally excited mode of methane is more likely to induce the dissociative chemical adsorption of methane.[2] Both of these modes are infrared-active modes, and can thus be excited by an infrared laser. The energy levels, lifetimes and decay characteristics of the methane vibrational modes have been extensively studied by C. B. Moore and coworkers[3] using a helium-neon infrared laser line which happens to overlap a vibrational level of the ν_3 state. Our experiment was designed to use the same technique to excite methane molecules in the vicinity of a rhodium surface into the ν_3 excited state. The resulting adsorption would be compared to that of unexcited (room temperature) methane. Then by deactivating this mode to the lowest excited vibrational level, ν_4, we can measure adsorption from this excited state. The deactivation would be accomplished by a high pressure ($\sim$1 torr) of helium gas, which would increase the molecular collision probability by several orders of magnitude.

The experiment would then proceed as follows:

A. Low Pressure (ν_3) Test

The methane will be admitted through a capillary doser to the laser cell. It will then be excited by a helium-neon infrared laser line at 3.39 μ. The configuration of the laser cell will allow the radiation to be reflected up to ten times in front of the crystal. After a variable time of excitation, the cell will be evacuated, and the thermal desorption spectrum of species left on the rhodium surface will be measured using a

quadrupole mass spectrometer. Hydrogen will be measured primarily, as it is the expected product of CH_4 dissociation.

B. High Pressure (ν_4) Test

This test will then be performed to compare with the former results. In addition to methane, approximately one torr of helium will be admitted to the laser cell prior to excitation. The helium pressure can be measured accurately with a capacitance manometer. The helium, 99.9999% pure to begin with, will have been purified to less than one part in 10^7 hydrogen impurities by diffusing through a heated quartz tube.

The methane will be excited as in the first experiment by shining the laser on the cell in the same multipass configuration. Because of the large number of collisions that the methane molecules undergo before reaching the crystal, they will have deactivated to the ν_4 vibrational mode. The cell will be evacuated and the flash desorption hydrogen signal will be recorded along with adequate controls, such as moving the crystal away from the region of laser excitation, performing the experiment without laser excitation, and performing the experiment without the crystal (to test for effects due to the crystal support wires). These two experiments should be sufficient to determine whether ν_3 or ν_4 is involved with overcoming the activation energy barrier to the dissociative chemisorption of methane on a cold rhodium surface.

The excitation energy of the ν_4 mode of methane is 1306 wave numbers which translates to 3.9 kcal/mole. Since the activation energy of chemisorption is measured to be $\sim 7 \pm 1$ kcal/mole, it is expected that translational energy is important to the process. If no adsorption is seen from either the ν_3 or the ν_4 mode, this will probably be the reason.

In that case we will heat the methane first to a temperature of about 400 - 500 K, at which temperature Stewart and Ehrlich still saw no dissociative adsorption, but which should be high enough to provide the necessary translational energy.

Construction of the System

Fig. 2 shows a schematic diagram of the final system. Two nickel getters will be used to purify the methane and one titanium getter will be used on the helium. Oxygen and hydrogen will be used for cleaning and calibration purposes.

The system construction involved an inordinately large number of technical problems. Several bakeout cracks forced the installation of glass bellows at every possible stress point. The system was initially designed with doubly trapped mercury diffusion pumps but one of these cracked off the system and contaminated the mass spectrometer with mercury, so it has been replaced by an ion pump. Because of the large number of setbacks, the experiments have yet to be performed. Preliminary data included the determination of the extinction coefficient of methane using our laser. Fig. 3 shows the data and a weighted least-squares regression line, giving an extinction coefficient of $\varepsilon = 0.13$ $torr^{-1}cm^{-1}$ compared with literature values of $\varepsilon = 0.12$ and $\varepsilon = 0.18$ $torr^{-1}cm^{-1}$.

Construction of the system and performance of the experiments will be continued by Dr. John T. Yates, Jr. and Jenna J. Zinck, both at Caltech and in Washington, D.C. at the National Bureau of Standards.

References

1. Stewart, C. N., and Ehrlich, G., J. Chem. Phys. 62 (1975) 4672-4682.

2. The reader is referred to my Ph.D. Candidacy report (March 1978) for a detailed description.

3. Moore, C. B., Acc. Chem. Res. 2 (1969) 103-109, and references therein.

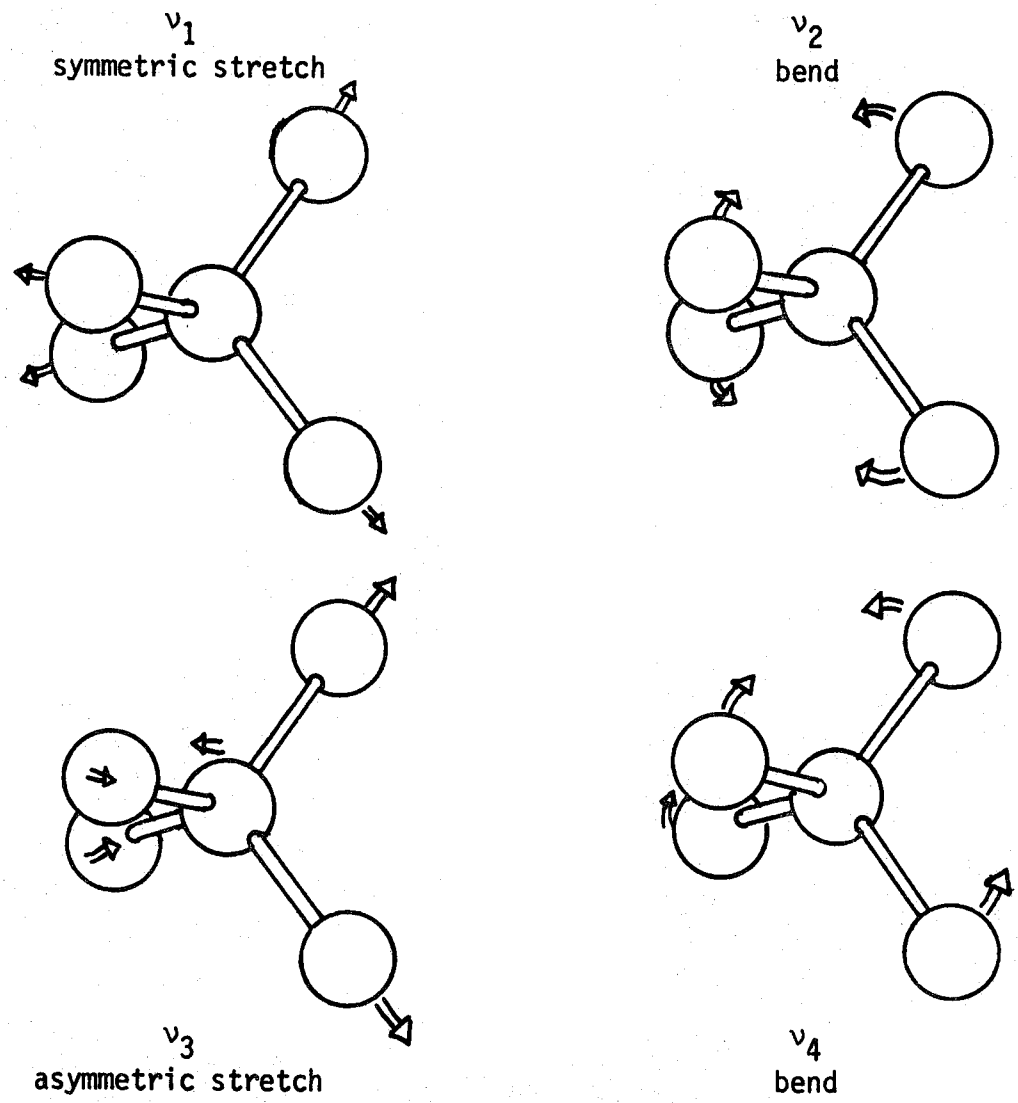

Figure 1. Vibrational modes of methane.

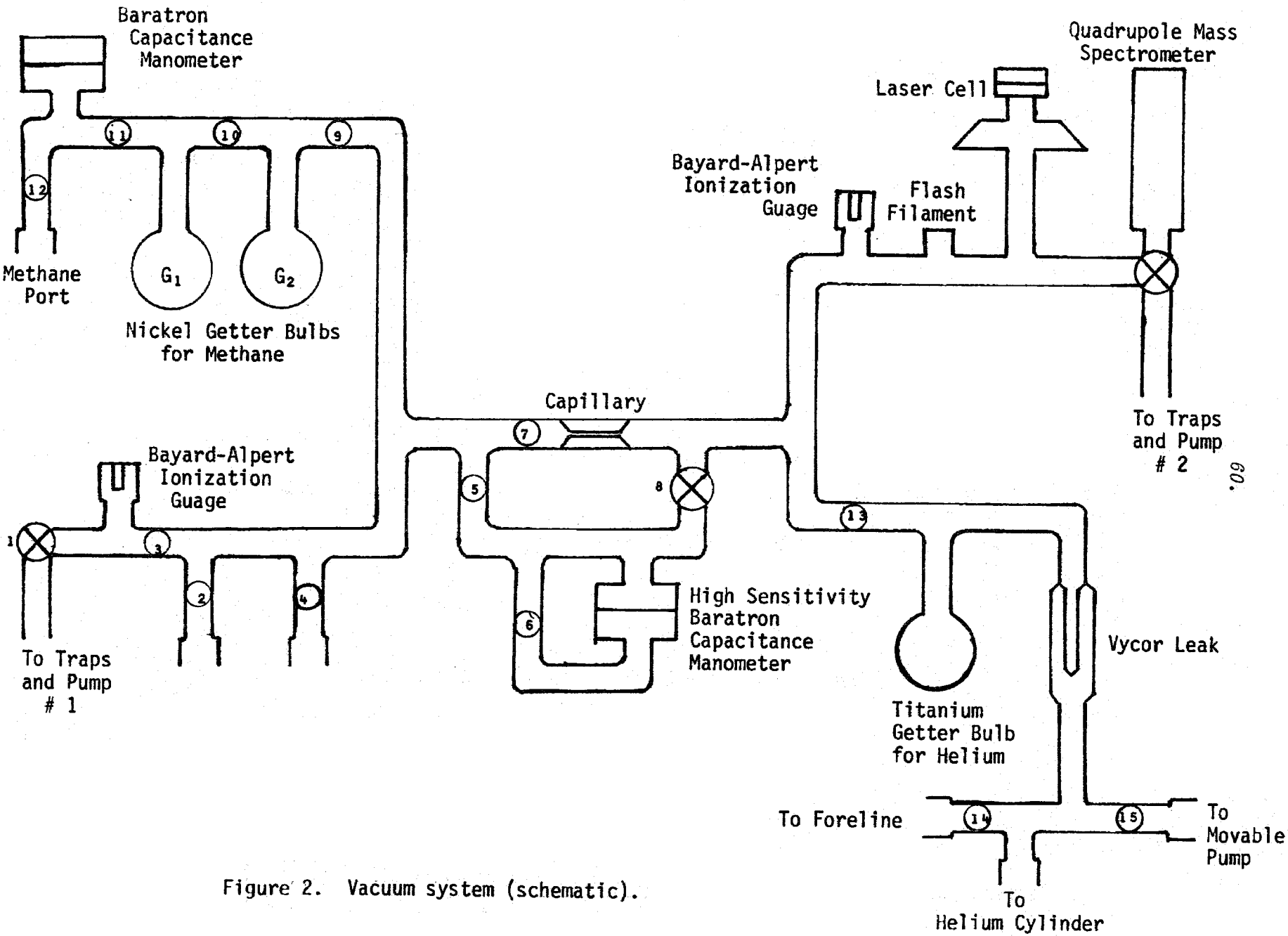

Figure 2. Vacuum system (schematic).

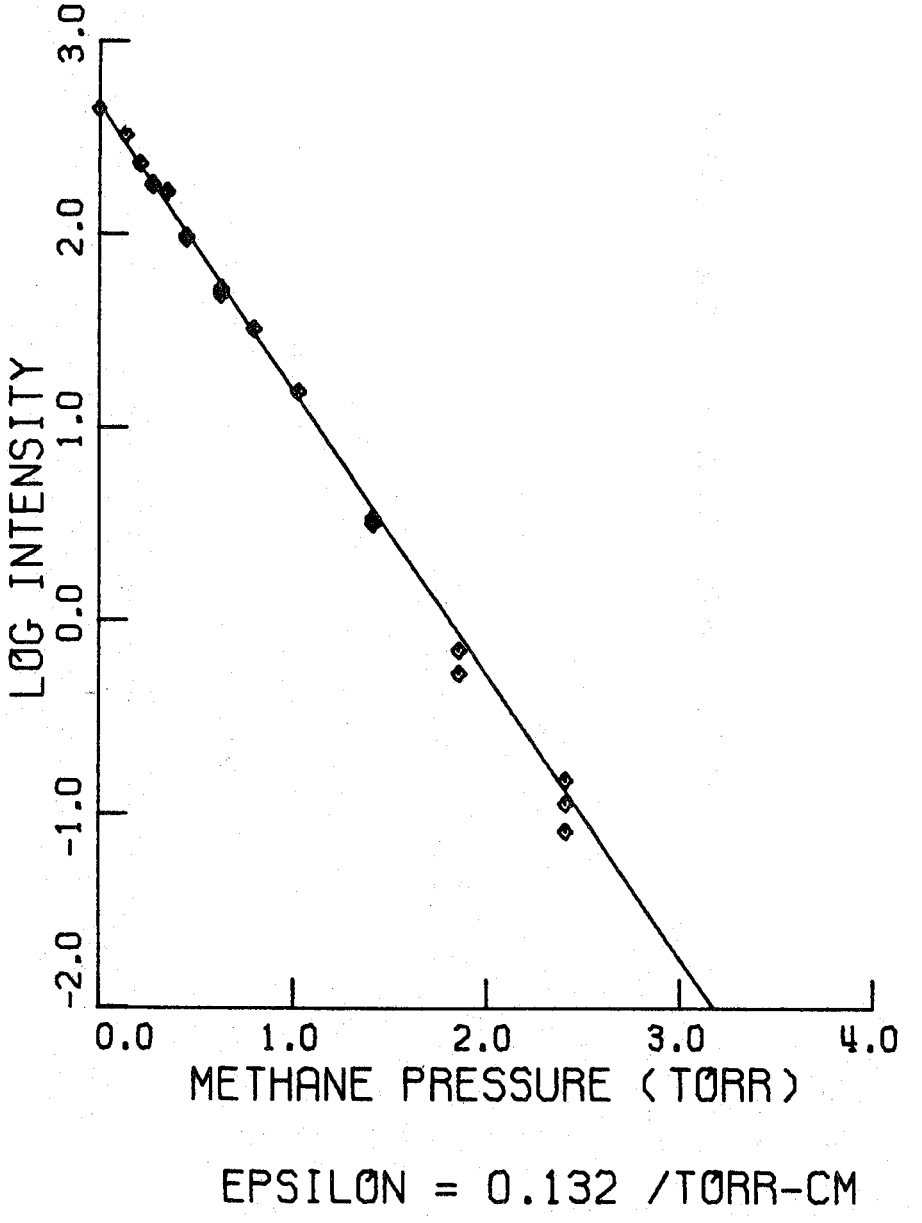

Figure 3. Extinction coefficient of methane.

APPENDIX 3

Propositions

1. Matrix Isolation of Metal-Silica Models.
2. A Hartree-Fock Model of Physical Adsorption.
3. Metal Carbonyl Complexes on Surfaces.

Proposition I

Metal catalysts are frequently dispersed as small particles in order to increase their surface areas and their per-atom efficiencies. For proper handling and recovery of the particles the catalysts must be attached to some sort of support material. Silica gel and other silicates are often used for this purpose because of their inertness to catalytic reagents, their ability to hold the catalyst, and often their ability to enhance the catalytic activity.[1, 2]

The importance of supported metal catalysts is an obvious motivation for research into the nature of the metal-silica bonding in supported heterogeneous catalysts. Much is known about the properties of the metal-silica bond in homogeneous systems (one or two metal atoms)[3] but corresponding information on larger systems such as clusters and particles does not exist.[4]

It is therefore proposed that a study be undertaken of the bonding between metal clusters and silica or silicates. The aims of such a study would be to describe as many different bonding parameters as possible, such as the geometry of such complexes (bond distances, and which atoms are involved in bonding), the effect on the bonding of other atoms bound to silicon, the relative numbers of support and metal atoms, and the effect of the support on adsorption (ligand-binding) properties of the metal. Of course no one technique can definitively answer all of these questions for even one system, but a technique which promises to give clues to some of them is cryophotoclustering or matrix isolation.

In matrix isolation experiments, the atoms whose properties are to be

studied are co-condensed in a matrix of inert gas atoms at low temperatures (10 - 77 K).[5 – 8] Gas phase spectra of the atoms are compared to the ultraviolet and optical, or infrared absorption spectra of the species in the matrix. As irradiation continues the matrix begins to heat up. Careful control of the wavelengths and intensities of irradiation allows one to follow new species as they are formed by the thermal diffusion of species inside the matrix. In this manner one can selectively study small clusters (one to about six atoms) of one[6] or two[5, 7] co-condensed species.

When choosing a system one must keep several questions in mind. Is the system relevant to current scientific studies? Will it be simple enough to understand, and is it interesting? A system which seems to fit these criteria is rhodium atoms and SiO molecules in an argon matrix. Rhodium is selected because of its catalytic importance[1, 2, 9 – 12] and because homogeneous solutions of complexed rhodium, both atoms[13 – 16] and clusters [4, 13, 17, 18] are well known. Optical spectra of the clusters, if they are not now available, should at least be fairly easy to obtain.

Silicon monoxide, SiO, is chosen as the model support species because it is intermediate between true support materials such as zeolites, which are too large to understand or possibly even to incorporate in such matrices, and silicon atoms, which would be simpler to study but are far different from support materials. Furthermore, SiO contains oxygen, which is frequently indicated as the atom through which metals bind to supports.[2, 19] It will be possible to study such interactions in this experiment.

Matrix trapping of the two species will be performed by heating them in separate furnaces. Rhodium wire will be wound around high melting tungsten wire and evaporated onto spectral plates such as NaCl (for optical

and ir experiments) and CsI (for ir studies).[8] Simultaneously, SiO will be formed by heating SiO_2 and Si to 1480 – 1680 K in an argon atmosphere.[20] All three gases will be deposited onto the cold plates. Concentration ratios will be varied over several orders of magnitude using the more dilute samples to study atomic absorptions and the more concentrated samples for clusters.

During the deposition process total amounts deposited can be monitored using a quartz crystal microbalance.[8] This consists of a 5 MHz quartz crystal oscillator which is exposed to the same deposition current as the spectral plates.[8] The rate of frequency change of the crystal is proportional to the added mass. By correcting for geometrical factors one can calculate the mass added to the spectral plate.

With the variables of concentration ratios, irradiation frequency, and irradiation time one can perform a large number of useful experiments. Some of the more straightforward types are listed in Table 1. One thing to bear in mind is that taking an absorption spectrum causes heating of the matrix in localized spots around the irradiated species. That species can then diffuse through the matrix if the heating is intense enough. By varying the time of irradiation one can control this effect.

As the species diffuse through the matrix they will form various types of chemical bonds. Since Rh–Rh bonds, Rh–SiO bonds and SiO–SiO bonds are stronger than any bonds to argon, one can expect to build larger clusters of these types as irradiation continues. By selective irradiation, say of rhodium atomic lines, one can heat the matrix around a rhodium atom until the atom moves to another Rh or SiO. The bonding will change the absorption frequency so that the newly formed cluster will no longer be able to diffuse. Thus the absorption due to rhodium atoms will decrease and absorptions due to clusters will increase with time. Note that the former lines can be

Table 1

	Concentrations Ar:Rh + SiO	Rh:SiO	Irradiate	
1.	1000:1	1:0	Rh	Rh atomic absorptions
2.	100:1	1:0	Rh	Rh atoms plus some Rh_2
3.	10:1	1:0	Rh	Rh atoms, some Rh_2 and higher clusters
4.	10:1	1:0	Rh_2 after Rh	Rh_2 disappearing Rh, Rh_n $n > 2$ growth
5.	10:1	1:0	Rh_n after Rh	Rh_n disappearing, others growing
6.	1000:1	0:1	SiO stretch	SiO vibrations
7.	1000:1	0:1	SiO optical bands	SiO electronic excitation
8 –11.	same as 2 - 5	0:1	SiO vibrations	Si_nO_n $n = 1$ and up clusters growing
12.	1000:1	10:1-1:1	Rh	May see some Rh-SiO perturbations
13.	100:1	1:1	Rh	Probably will see Rh-SiO perturbations; Rh_2SiO, maybe.
14.	10:1	1:1	Rh	Probably will see Rh-SiO perturbations, Rh_nSiO clusters growing
15.	1000:1	1:1-1:10	SiO	May see Rh-SiO perturbations
16.	100:1	1:1	SiO	Probably see Rh(SiO), maybe $Rh(SiO)_2$
17.	10:1	1:1	SiO	Probably see $Rh(SiO)_n$
18.	100:1	10:1-1:10	Rh then SiO	See $Rh_nSiO \rightarrow Rh_n(SiO)_m$
19.	10:1	10:1-1:10	SiO then Rh	See $Rh(SiO)_n \rightarrow Rh_m(SiO)_n$
20.	100:1 or 10:1	10:1-1:10	Rh-SiO	Study M-SiO bond stretch, determine if M-SiO or M-O

continuously monitored while the latter absorptions must be measured in short pulses, or one would heat the clusters as well.

Both conventional lamps[6, 7] and lasers[8] have been used as light sources in cryophotochemical experiments. In addition to ir and uv/optical studies, laser Raman experiments have proved useful.[8] Raman spectroscopy is advantageous in that different selection rules allow transitions which are symmetry-forbidden in infrared absorption experiments. This allows a more complete characterization of the vibrational bands of the species formed. Since Raman experiments are technically more complicated than absorption experiments, it is recommended that these be postponed until after the corresponding ir and uv/optical data is understood.

It is expected that the proposed experiments will be able to answer a number of questions about the Rh–SiO system. Rates of formation of various rhodium clusters will be calculated, giving an indication of the activation energies involved. Thermodynamic stabilities can be inferred from the products obtained after extensive irradiation. Vibrational frequencies can be measured, and they will help determine the structures of the $Rh_n(SiO)_m$ complexes, indicating how the SiO molecules are bound to each other and to rhodium.

Other metals can be studied using cryophotoclustering, as can models for other support materials such as alumina. This technique promises a wealth of basic information about bonds characteristic of supported metal catalysts. It is hoped that in the long run this information will help predict more efficient and useful catalytic procedures.

References

1. Takahashi, N., Okura, I., and Keii, T., J. Mol. Catal. 3 (1977) 277 - 283.
2. Anderson, J. R., Structure of Metallic Catalysts. Academic, San Francisco, 1975.
3. Ellis, J. J., Organometal. Chem. 86 (1975) 1 - 56.
4. Smith, A. K.; and Basset, J. M., J. Mol. Catal. 2 (1977) 229 - 241.
5. Ozin, G. A., Power, W. J., Upton, T. H., and Goddard, W. A., III, to be published.
6. Klotzbücher, W. E., Mitchell, S. A., and Ozin, G. A., Inorg. Chem. 16 (1977) 3063 - 3070.
7. Ozin, G. A., Huber, H., and McIntosh, D., Inorg. Chem. 16 (1977) 3070 - 3078.
8. Kündig, P., Moskovitz, M., and Ozin, G. A., J. Mol. Structure 14 (1972) 137 - 144.
9. Brinen, J. S., Acc. Chem. Res. 9 (1976) 86 - 92.
10. Conan, J., Bartholin, M., and Guyot, A., J. Mol. Catal. 1 (1976) 375 - 382.
11. Bartholin, M., Graillat, C. H., Guyot, A., Coudurier, G., Bandiera, J., and Naccache, C., J. Mol. Catal. 3 (1977) 17 - 32.
12. Michalska, Z. M., J. Mol. Catal. 3 (1977) 125 - 134.
13. Baird, M. C., Progr. Inorg. Chem. 9 (1968) 1 - 159.
14. Cotton, F. A., Chem. Soc. Revs. 4 (1975) 27 - 53.
15. Dror, Yi, and Manassen, J., J. Mol. Catal. 2 (1977) 219 - 222.
16. Spek, T. G., and Scholten, J. J. F., J. Mol. Catal. 3 (1977) 81 - 100.
17. Chini, P., Longoni, G., and Albano, V. G., Adv. Organometal. Chem. 14 (1976) 285 - 344.
18. Anderson, J. R., Elmes, P. S., Howe, R. F., and Mainwaring, D. E., J. Catal. 50 (1977) 508 - 518.
19. Morrow, B. A., J. Phys. Chem. 81 (1977) 2663 - 2666.
20. Kozhevnikov, G. N., Izv. Akad. Nauk., SSSR, Metal. 4 (1972) 82 - 85.

Proposition 2

Physical adsorption of a molecule on a metal surface is due to a number of interactions, such as van der Waals, ionic and dipole attractions, in which the interaction energies are very low.[1] Typical physisorption bond strengths are less than about 5 kcal/mole. It is instructive to study physical adsorption theoretically in order to understand the changes in the electronic structure of the surface and the admolecule which lead to a stabilization energy of that magnitude.

Many theoretical models of physical adsorption have been studied. In the jellium model the metal surface is treated as a sea of electrons in a neutralizing background, and the effects of the field due to this surface on the orbitals of nearby adparticles are calculated. This method is not applicable to stronger bonds which involve mixing of surface and admolecule orbitals because the metal is treated in a highly approximate manner.

In a more exact manner one can treat the surface using Green's function expressions for the metal density of states.[2] Limitations in computational facilities then force a more approximate description of the admolecule; the reference cited uses one nondegenerate energy level per adatom.

I would like to propose a type of physisorption calculation in which metal orbitals and admolecule orbitals are treated with more nearly equal degrees of accuracy. Furthermore this scheme allows a detailed description of the bond character in that it separates out the interactions due to intermolecular charge transfer, intramolecular orbital polarization, purely electrostatic contributions, and quantum mechanical effects such electronic exchange and coupling. As the molecule moves closer to the surface, changes

in its structure can be quantitatively described and broken down into the several types of contributions. Insight of this sort can lead to paradigms for the electronic properties of physisorbed states and hence will contribute to a basic understanding of adsorption bonds.

The Energy Decomposition Method

The technique has been outlined in a series of papers by Morokuma and co-workers.[3 – 5] They describe a method which uses the Hartree-Fock LCAO-MO description of two isolated systems as a starting point and calculates the interaction of these two systems using Hartree-Fock theory. By isolating different terms in the interactional Fock matrix, they optimize the energy of the complex while allowing only one type of interaction to occur at a time.

For example, a system of two isolated molecules which are allowed to approach each other is represented by A + B → AB. To calculate the electrostatic interaction energy a Hartree-Fock calculation is performed in which no orbitals of A are allowed to mix with B orbitals (in other words, all overlap matrix elements of this sort are set to zero during the calculation). The energy calculated is the energy of the two subsystems at infinite separation (zero-order energies) plus internuclear repulsion and the attraction of each nucleus to the (zero-order) electron density of the other molecule. Nuclear repulsion and electron-nuclear attraction are calculated at some finite distance, usually the equilibrium bond distance. Polarization energy can be calculated by letting the occupied and vacant orbitals of each subsystem mix, but not allowing inter-system mixing. Such an energy contains zero order, electrostatic, and polarization terms; polarization energy is obtained by subtraction. Similarly charge transfer is calculated allowing the occupied

orbitals on each system to mix with the vacant orbitals on the other. Exchange energies are calculated by allowing occupied or vacant orbitals on each system to mix with the occupied or vacant orbitals, respectively, on the other system. Finally, the coupling error among these different contributions is evaluated by performing a calculation which allows all terms, and subtracting the sum of the individual interactions energies from this total interaction energy. Figures 1 and 2 diagram these calculations.

The coupling term serves the useful purpose of indicating the reliability of the calculations. For strong bonds, such as chemisorption bonds, this coupling term will generally be very large, indicating that tnis energy decomposition scheme is not valid.[6] This will happen when the bond distorts the initial subsystems so greatly that their zero-order states become meaningless in the complex. Because physical adsorption is a weak interaction, comparable in magnitude to others which have been studied by this technique (such as hydrogen bonds[5] and electron donor/acceptor complexes,[3] it is expected that the technique will work similarly well for physisorption.

Proposed System

A proper model for a physisorption system must include a metal and an admolecule. However, these subsystems are constrained to have small sizes because the computing facilities required grow as n^4 where n is the total number of orbitals involved. Two choices are possible for the metal: use a small metal atom such as beryllium, or approximate the orbital structure of a large one such as nickel using pseudopotentials to represent core orbitals. (In both cases the total number of atoms must be limited to three or four.) Although the second approach is quite useful much work has already been done in the area[7] and I shall focus on the first approach.

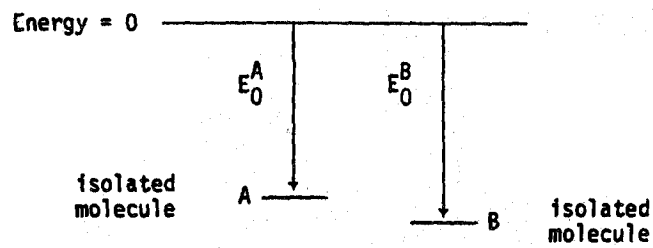

$E_0 = E_0^A + E_0^B$ = zero-order Hartree-Fock energy for the system.

ES = energy stabilization due to electrostatic interactions.

PL = polarization stabilization energy.

CT = charge transfer stabilization energy

EX = stabilization due to electron exchange.

MIX = coupling term.

Total Energy $= E_{total} = ES + PL + CT + EX + MIX + E_0$

(Sign convention: + for stabilization)

Figure 1. Zero-order energies.

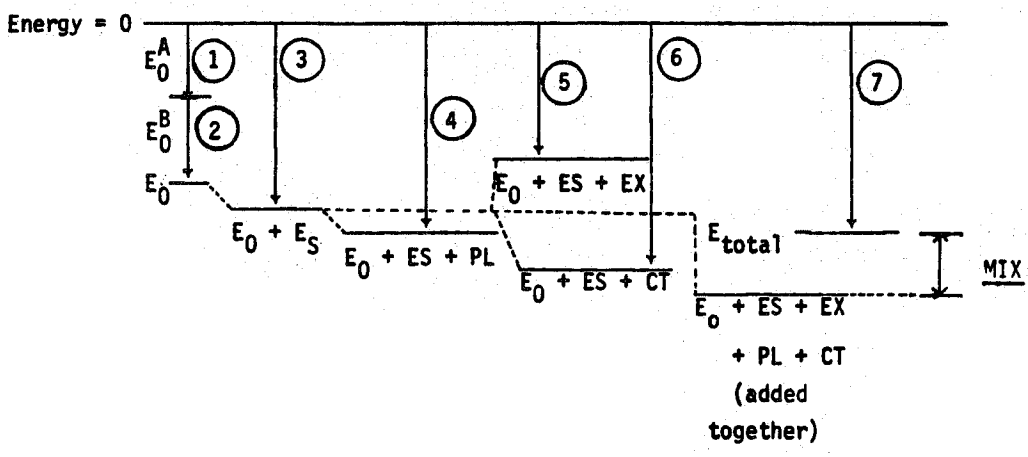

Calculation	Allows
(1)	Hartree-Fock convergence on isolated system A.
(2)	Hartree-Fock convergence on isolated system B.
(3)	Addition to sum of 1 and 2 of electrostatic interactions (calculated classically).
(4)	Hartree-Fock convergence allowing $A_{occ} \longleftrightarrow A_{vac}$ and $B_{occ} \longleftrightarrow B_{vac}$ mixing.
(5)	Hartree-Fock convergence allowing $A_{occ} \longleftrightarrow B_{occ}$ and $A_{vac} \longleftrightarrow B_{vac}$ mixing.
(6)	Hartree-Fock convergence allowing $A_{occ} \longleftrightarrow B_{vac}$ and $A_{vac} \longleftrightarrow B_{occ}$ mixing.
(7)	Hartree-Fock convergence on system AB (allows all types of mixing).

Figure 2. Energy Decomposition

One must select a system that represents a true physisorption situation as closely as possible, under the constraints of the model. For this reason I choose to study the interaction of Be_2 with CO and O_2. The surface chemistry of beryllium has not been studied much, presumably because of the metal's cost as well as its low catalytic activity; but some useful generalizations should be available from the study of its interaction with typical ligands. CO is probably the most studied admolecule of all (with the possible exception of hydrogen) and O_2 is not far behind. One should be able to compare the isolated structures of these ligands with their interacting structures using the energy decomposition method.

Several geometries must be studied, not only to determine which configuration is energetically most stable but also what changes occur in the molecule to make that geometry most favored. Figure 3 shows some reasonable configurations to start with. In all cases the bond lengths between the metal and the ligands can be optimized for the most stabilization. It would also be interesting to calculate the most stable C–O and O–O bond lengths in the most favored geometries. All these energies are total interaction energies. Once the best geometry is calculated one then "decomposes" the total energy by repeating the calculation with selected mixing terms set to zero (not allowed). By performing calculations numbered 3 through 6 in Figure 2, (1, 2 and 7 were done previously) one subtracts to get the decomposed energies.

Perhaps the most useful presentation of the data in these calculations entails electron density maps. In these maps one plots the change in electron density which occurs in the two subsystems as they approach each other. Such maps are commonly made for the total energy contribution, but this scheme allows one also to plot changes incurred by individual energy contributions. It is computationally easy to obtain these maps since each Hartree-Fock

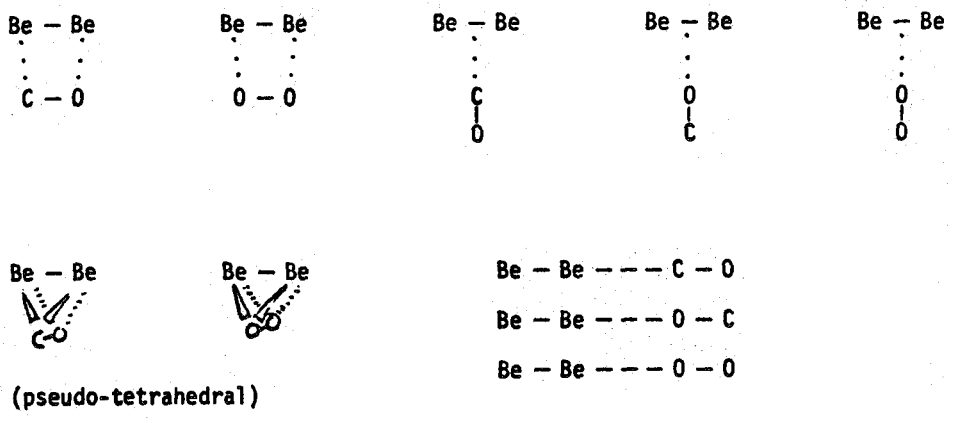

Figure 3. Bonding geometries to test.

calculation derives molecular orbitals as well as energies. The electron density at any point is simply the sum of probabilities that an electron will be at that point for each orbital.

Some electron density maps are shown in Figure 4.[3] These came from a calculation of the interaction of CO with BH_3. As an example of the chemical usefulness of these calculations, I show the charge transfer maps for both forward ($H_3B \rightarrow CO$) and backward ($CO \rightarrow BH_3$) electron donations. Note that in the second case CO loses π-electron density (dotted lines) which BH_3 gains in the vacant boron lone pair orbital. It would be very interesting to see similar maps for ligand-to-metal interactions, both for the proposed model and for heavier metals (using pseudopotentials). I strongly suggest such calculations be performed.

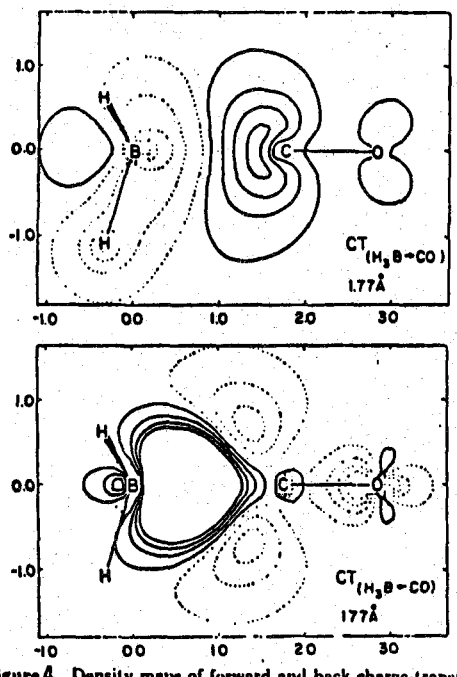

Figure 4. Density maps of forward and back charge-transfer components for the complex OC-BH_3 at R(C–B) = 1.77 Å in the C_{3v} approach. Contours indicated are, successively, ±0.5, ±2.0, ±3.5, ±5.0 × 10^{-3} $bohr^{-3}$.

Figure 4. From Reference 3.

References

1. Clark, A., The Theory of Adsorption and Catalysis. Academic, New York, (1970).

2. Ho, W., Cunningham, S. L., and Weinberg, W. H., Surf. Sci. 62 (1977) 662 - 674.

3. Morokuma, K., Acc. Chem. Res. 10 (1977) 294 - 300, and references therein.

4. Kitaura, K., Morokuma, K., Int. J. Quant. Chem. 10 (1976) 325 - 340.

5. Morokuma, K., J. Chem. Phys. 55 (1971) 1236 - 1244.

6. K. Morokuma, personal communication.

7. Goddard, W. A., III, to be published.

Proposition 3

ABSTRACT

Metal carbonyl complexes, specifically $Ni(CO)_4$ and later large metal cluster complexes, are to be adsorbed on single crystal surfaces, specifically copper. Ultraviolet photoemission spectroscopy will be used to monitor the dissociation of carbonyl groups from the nickel atoms. Tip angles of the carbonyls still attached to nickel can be measured using angle-resolved photoemission spectroscopy. From the change in these angles with time and temperature, one can calculate ligand repulsions and dissociation activation energies. Other techniques also allow the calculation of relative adsorption bond strengths between different adsorption sites.

Introduction

Homogeneous and heterogeneous catalysis are more closely related than is usually acknowledged. Homogeneous catalysts are easier to characterize and to modify by means of exchanging ligand groups. They are also efficient in that every metal atom is available to the reagents.

Heterogeneous catalysts are prepared so as to maximize the proportion of active, surface atoms while retaining the advantages of separability and stability. It is important to investigate both types as well as to create and study new forms of catalysts.

Recently, transition metal cluster compounds have shown increasing industrial applicability.[1] It is important to research such cluster compounds

as intermediates between homogeneous and heterogeneous catalysts. In particular, it is desirable to study the changes that occur in atomic properties of metal atoms as the compounds range from mononuclear complexes through small[2] and large[3 - 4] clusters to particles and single crystal surfaces. At present, there are few techniques which can be suitably applied to all catalyst forms. Homogeneous catalysts are most frequently characterized by their infrared absorptions and Raman spectra,[5] certain electrochemical redox reactions,[6] and other spectroscopies.[7 - 9] These techniques can give information about the geometries, vibrational force constants, electronic structures and chemical reactivities of the complexes. Many of these techniques cannot, however, be applied to single-crystal surface studies, which are carried out in ultrahigh vacuum conditions. Using surface techniques one can deduce similar information about heterogeneous catalytic species: electron diffraction indicates surface ordering which can imply adatom interaction; photoemission and work function studies can describe surface-induced electronic structure and admolecule geometries; vibrational spectroscopies can determine structures and force constants; and thermodynamic and kinetic stabilities and chemical reactivities can be calculated from temperature-dependent effects.

It is proposed that these surface techniques be used to study the gradual change in many molecular properties as one examines homogeneous catalysts, cluster compounds, metal particle and single crystal surfaces. These properties include preferred binding sites of ligands (adatoms), such as bridged, terminal or low-symmetry; the optimum number of ligands per metal atom, and bond lengths and angles between them; bond energies; internal structural changes in the ligands; and electronic structural changes in the metal atoms. For example, how do the electronic and

vibrational structures of carbon monoxide vary between gaseous molecules, physically and chemically adsorbed molecules and cluster and mononuclear metal complex carbonyls?

Proposed Experiment

I propose that the change in molecular properties of metal carbonyls be followed as additional metal atoms are added to a mononuclear complex. One can adsorb metal carbonyls on well-oriented, single-crystal surfaces and study the subsequent behavior of the carbonyl moieties with ultraviolet photoemission spectroscopy and other surface techniques.

The first experiment of this type should employ a volatile, easily obtainably metal carbonyl and a compatible surface. Nickel carbonyl ($Ni(CO)_4$), with a boiling point at atmospheric pressure of 316 K , is a suitable admolecule.

A logical first choice for the substrate would be a single crystal plane of nickel. If such a surface were ideal, with no imperfections or steps, this substrate would give useful information. In this case a nickel atom would bind to the nickel substrate through d-electron interactions, pushing the carbonyls away from the substrate nickel atoms. If more than one carbonyl remained attached to the original nickel atom, the carbonyls would not be oriented perpendicular to the surface, and the angular distribution of ultraviolet photoelectrons might be able to measure this "tipping" effect. Heating the crystal would initiate surface diffusion of these carbonyls and the photoemission patterns would revert to those of CO on a flat nickel surface.

However, it is not currently possible to prepare such an atomically flat surface. In the case of an imperfect surface the small number of

added nickel atoms with attached carbonyls is likely to be insignificant relative to the number of substrate nickel atoms which adsorb carbonyls from other sources (such as those lost when a $Ni(CO)_4$ molecule dissociatively adsorbs elsewhere). It would be better to choose a surface whose effects would be separable from those of the added molecule. Copper binds CO in an entirely different manner from nickel: the adsorption bond strength is about one-third lower, so at room temperature less CO remains adsorbed on copper than nickel.[11] Furthermore, since the work functions of clean copper and nickel differ by as much as 3 - 4 eV,[12] the photoemission spectrum of the surface should show distinct peaks for CO on copper and CO on nickel. One could monitor the nickel CO peak intensity to measure how much CO remains on nickel as a function of time and temperature. At low temperatures the CO that leaves will move to other sites on the copper surface, whereas at higher temperatures (around 300 K and above) the carbonyl is likely to desorb altogether. One can monitor total CO photoemission intensities to distinguish which effect is occurring under any given conditions.

Copper is a good substrate for another reason: bimetallic clusters of copper and nickel have been studied by chemisorption and activity measurements,[13] providing a basic understanding of the interactions between the two metals. The proposed experiment will both utilize and help clarify these conclusions about the chemisorption properties of nickel atoms on copper.

The experiment will proceed as follows:

1. A clean copper single-crystal surface will be prepared using standard techniques.
2. $Ni(CO)_4$ will be admitted to the vacuum chamber for specific exposure times.

3. Ultraviolet photoemission spectra, both angle-integrated and angle-resolved, will be taken of the surface as a function of time at constant temperature for several temperatures in the range 90 - 300 K.
4. Low-energy electron diffraction (LEED) patterns and their intensity vs. voltage curves will be measured under several conditions.
5. After each experiment the crystal will be flashed to high temperatures and the thermal desorption of surface species will be measured using a quadrupole mass spectrometer.

From the temperature dependence of angle integrated photoemission intensities due to CO on nickel, one can calculate activation energies of dissociation of the surface nickel carbonyl species. The angular distributions of these photoelectrons can be compared to distributions calculated theoretically[14] for CO molecules tipped away from vertical at various average tip angles. The best fit will determine the equilibrium positions of the carbonyl ligands relative to the other ligands and to the surface. As the temperature is raised more CO's are expected to move away from the nickel atoms and the remaining ones will stand up more vertically.[15] Desorption energies calculated from thermal desorption peak temperatures will suggest models for the surface species. Finally, LEED data will be studied to determine surface ordering of $Ni(CO)_4$ and CO, especially as carbonyls dissociate from the nickel atoms.

This study as outlined above will determine the feasibility of studying metal carbonyl complexes on a surface. With luck one will then be able to adsorb larger clusters on metal surfaces. With clusters such as $Rh_6(CO)_{16}$ one may be able to distinguish carbonyls attached to the cluster even when the substrate used is also rhodium. This would be a useful way

to study chemisorption properties of metal edges, corners and imperfections, represented by the metal clusters, relative to flat surfaces, represented by the substrate. In the meantime it would be quite interesting to study small metal complexes on different surfaces.

References

1. Smith, A. K. and Basset, J. M., J. Mol. Catal. 2 (1977) 229-241.

2. Chini, P., Longoni, G., and Albano, V. G., Adv. Organometal. Chem. 14 (1976) 285-344.

3. Anderson, J. R., Elmes, P. S., Howe, R. F., and Mainwaring, D. E., J. Catal. 50 (1977) 508-518.

4. Primet, M., Basset, J. M., Garbowski, E., and Mathieu, M. V., J. Am. Chem. Soc. 97 (1975) 3655-3659.

5. Ozin, G. A., Acc. Chem. Res. 10 (1977) 21 - 26.

6. Ferguson, J. A., and Meyer, T. J., J. Am. Chem. Soc. 94 (1972) 3409 - 3412.

7. Frankel, R. B., Ruff, W. M., Meyer, T. J., and Cramer, J. L., Inorg. Chem. 13 (1974) 2515 - 2517.

8. Barber, M., Vickerman, J. C., and Wolstenholme, J., J. Catal. 42 (1976) 48 - 53.

9. Thomas, M. G., Pretzer, W. R., Beier, B. F., Hirsekovn, F. J., and Muetterties, E. L., J. Am. Chem. Soc. 99 (1977) 743 - 748.

10. Cotton, F. A., and Wilkinson, G., Advanced Inorganic Chemistry, 3rd ed., Interscience, New York, 1972.

11. There exists some controversy over the nature of CO adsorption on copper at room temperature. See Isa, S. A., Joyner, R. W., and Roberts, M. W. J. Chem. Soc.: Faraday Trans. I, 74 (1978) 546-554; Chesters, M. A., and Pritchard, J., Surf. Sci. 28 (1971) 460-468; Tracy, J. C., J. Chem. Phys. 56 (1972) 2748-2754; and Joyner, R. W., McKee, C. S., and Roberts, M. W., Surf. Sci. 26 (1971) 303-309.

12. Cu: 8-9 eV; Kittel, C. Introduction to Solid State Physics 5th edition, Wiley, New York (1976) p. 154. Ni: 4-5 eV, Chemical Rubber Company handbook, 53rd edition, CRC press: Cleveland (1973) p. E 70.

13. Sinfelt, J. H., Acc. Chem. Res. 10 (1977) 15-20.

14. Davenport, J. W., Phys. Rev. Lett. 36 (1976) 945-949.

15. Andersson, S., Solid State Commun. 21 (1977) 75-81.